https://doi.org/10.5194/amt-2020-81
Preprint. Discussion started: 15 April 2020

Atmospheric Measurement Techniques Discussions

The quantification of NOx and SO_2 point source emission fluxes errors of mobile DOAS on the basis of the Gaussian dispersion model: A simulation study

Yeyuan Huang[1,2], Ang Li[1], Thomas Wagner[4], Yang Wang[4], Zhaokun Hu[1], Pinhua Xie[1,2,3], Jin Xu[1], Hongmei Ren[1,2], Xiaoyi Fang[5], Bing Dang[6]

[1]Key Lab. of Environmental Optics and Technology, Anhui Institute of Optics and Fine Mechanics, Chinese Academy of Sciences, Hefei, 230031, China.

[2]University of Science and Technology of China, Hefei, 230027, China.

[3]CAS Center for Excellence in Regional Atmospheric Environment, Institute of Urban Environment, Chinese Academy of Sciences, Xiamen, 361000, China.

[4]Max Planck Institute for Chemistry, Mainz, Germany.

[5]Chinese Academy of Meteorological Science, Beijing, 100081, China.

[6]Beijing Municipal Climate Center, Beijing, 100089, China.

Correspondence to: Ang Li(angli@aiofm.ac.cn), Pinhua Xie (phxie@aiofm.ac.cn) and Yang Wang(y.wang@mpic.de)

Abstract: Mobile differential optical absorption spectroscopy (mobile DOAS) has become an important tool for the quantification of emission sources, including point sources (e.g., individual power plants) and area emitters (e.g., entire cities). In this study, we focused on the error budget of mobile DOAS measurements from point sources, and we also offered recommendations for the optimum settings of such measurements. First we established a Gaussian plume model from which the NOx and SO_2 distribution from the point source was determined. In a second step the simulated distributions are converted into vertical column densities of NOx and SO_2 according to the mobile DOAS measurement technique. With assumed parameters, we then

https://doi.org/10.5194/amt-2020-81
Preprint. Discussion started: 15 April 2020


Atmospheric Measurement Techniques Discussions

drove the forward model in order to simulate the emissions, after which we performed the analysis. Following this analysis, we conclude that: **(1)** Larger sampling resolution clearly results in larger flux error. The proper resolution we suggest is between 5 m and 50 m. Even larger resolutions may also be viable, but > 100 m is not recommended. **(2)** Error effects vary with measurement distance from the source. We found that undetectable flux (measured VCDs are under the detection limit) is the main error source when measuring far from the source, for both NOx and SO_2. When measuring close to the source, low sampling frequency results in large flux error. **(3)** The wind field primarily affects 2 aspects of the flux measurement error. When measuring far from the source, dispersion results in more undetectable flux, which is the main error source. When measuring close to the source, wind field uncertainty becomes the main error source of SO_2 flux, but not of NOx. We suggested that the proper wind speed for mobile DOAS measurements is between 1 m/s and 4 m/s. **(4)** The study of NOx atmospheric chemistry reactions indicated that a [NOx]/[NO_2] ratio correction has to be applied when measuring very close to the emission source. But even when such a correction is applied, the remaining errors can be significant. To minimize the [NOx]/[NO_2] ratio correction error, we recommended 0.05 NO_2 maximum reaction rate as the accepted NOx steady-state thus to determine the proper starting measurement distance. **(5)** The error of the spectral retrieval is not a main emission flux error source and its error budget varies with the measuring distance. **(6)** Increasing the number of measurements can lower the flux error that results from wind field uncertainty and retrieval error. This directly indicates that SO_2 flux error could be lowered if the measurements are repeated when not too far from the emission source. With regard to NOx, more measurement times can only work effectively when not very close or too far from the source. **(7)** Also the effects of the temporal and spatial sampling are investigated. When the sampling resolution is prescribed, the integration depends on the driving speed and the corresponding flux error is mainly determined by the undetectable flux. When the car speed is prescribed, the integration time is determined by the sampling resolution for measuring near the source, while undetectable flux predominates when far away. **(8)** As a general recommendation, our study suggests that emission rates < 30 g/s for NOx and < 50 g/s for SO_2 are not recommended for mobile DOAS

https://doi.org/10.5194/amt-2020-81
Preprint. Discussion started: 15 April 2020


Atmospheric Measurement Techniques Discussions

measurements. The source height affects the undetectable flux, but has little influences on the total error.

Based on the model simulations our study indicates that mobile DOAS measurements are very well suited tool to quantify point source emissions. The results of our sensitivity studies are important to make optimum use of such measurements.

1 Introduction

Nitrogen oxides (NOx = NO + NO_2) and sulphur dioxide (SO_2), poisonous and harmful trace gases in the atmosphere, are critical participants in tropospheric chemical reactions (Seinfeld and Pandis, 1998; Beirle et al., 2003). NOx and SO_2 are emitted into the atmosphere via natural and anthropogenic emissions, especially from traffic and industries. In recent years, China has experienced large areas of haze pollution, which have drawn worldwide scrutiny due to their NOx, SO_2, and VOC content, although strict policies designed to control the emission of pollution gases have been implemented (Richter, et al., 2005; Ding et al., 2015; Jin et al., 2016). It is of great significance to study gas emission pollution both qualitatively and quantitatively.

Differential Optical Absorption Spectroscopy (DOAS) is a technique developed in the 1970s that focuses on the telemetering of atmospheric gases, particularly trace gases (Platt and Stutz, 2008). After years of research, various types of DOAS technology have been comprehensively developed, including LP-DOAS, MAX-DOAS, and mobile DOAS.

Mobile DOAS technology was originally used to measure volcanic SO_2 emissions (Bobrowski et al., 2003; Edmonds et al., 2003; Galle et al., 2003), and it was then developed to measure the NO_2 and SO_2 emission fluxes from industrial parks (Johansson et al., 2006). In 2008, Mattias Johansson used a mobile mini-DOAS device to quantify the total emission of air pollutants from Beijing and evaluated the measurement error, mainly in terms of the uncertainties in the wind field, experimental setup, sunlight scattering in the lower atmosphere, and retrieval error. During the MCMA 2006 field campaign, C. Rivera et al. (2009) used a mobile mini-DOAS instrument to measure the NO_2 and SO_2 emissions of the Tula industrial complex in Mexico and also estimated the flux error. In O. Ibrahim et al. (2010), T. Wagner et al. (2010),

https://doi.org/10.5194/amt-2020-81
Preprint. Discussion started: 15 April 2020


Atmospheric Measurement Techniques Discussions

and R. Shaiganfar et al. (2011, 2017), air mass factor (AMF), sampling resolution, NOx chemical reactions, and atmospheric lifetime were introduced in order to analyze the emission flux error. The analysis of emission flux error sources has gradually come to focus on the wind field uncertainty, sampling resolution measurement error (GPS error), Slant Column Density (SCD) retrieval error, AMF error, and other error sources. The aforementioned studies primarily concentrated on regional/industry park emission fluxes, as opposed to point sources.

Different from regional/industry park measuring, point source emission flux can be measured in diverse ways, with different measuring distances, varying sampling resolutions, and so on. Therefore, the error sources and influence factors affecting the flux measurements are different. In order to investigate the impact of these factors and thereby recommend optimum settings for point source flux measuring using mobile DOAS, we performed an in-depth study on the effects of error sources and influence factors on point source emission flux measuring.

There are innate deficiencies in the experimental method used to analyze the emission flux error since there are so many scenarios that need to be verified, and the various factors cannot be well controlled during experiments. Therefore, a convenient way to assist the analysis is sorely needed. In the absence of precise requirements, the simulation method is a good alternative for facilitating the analysis of mobile DOAS emission flux error, given its convenience and feasibility.

Using a model based on Gaussian plume dispersion and the mobile DOAS emission flux measurement method, we here performed a simulation to study the measurement of NOx and SO_2 point source emission flux.

This paper is organized as follows: In Section 2, the methodological framework is presented. In Section 3, the parameters used to drive the simulation are delineated. Section 4 describes the simulation performance and data analysis, Section 5 presents our conclusions, and the Appendix displays the overall simulation results.

https://doi.org/10.5194/amt-2020-81
Preprint. Discussion started: 15 April 2020

Atmospheric Measurement Techniques Discussions

2 Methodology and forward model

2.1 Overview of methodology

Since individual experiments take place in complex and variable scenarios, in order to investigate the error sources and influence factors that impact the flux measurement error, typical mobile DOAS measurements of the NOx and SO_2 emission fluxes were modeled with the following assumptions:

(1) NOx and SO_2 gas continuously exhaust from an isolated and elevated point source at the position (0 m, 0 m, 235 m). The plume rises approximately 15 m.

(2) The topography around the point source is flat and the background concentration of the pollutants is 0.

(3) Air turbulence is constant in space and time.

(4) A zenith-sky mobile DOAS measures the gas underneath the plume in the *y*-direction at around noon (see Figure 1). Spectra, GPS data, and wind profiles are available for individual measurements.

(5) The sunlight radiance received by the mobile DOAS instrument is stable.

Figure 1 presents the schematic diagram of the modeled mobile DOAS measurement of a point source.

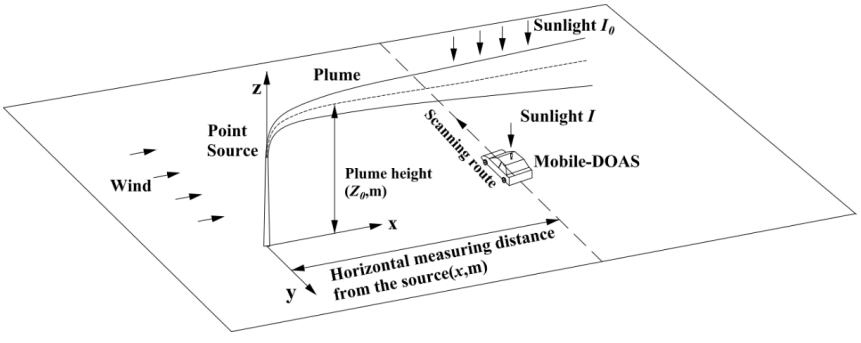

Figure 1. Schematic diagram of the modeled mobile DOAS measurement underneath the plume

Based on the performance of typical mobile DOAS measurements, a forward model of flux calculations was generated and error analysis performed according to the forward model, as shown in Figure 2.

https://doi.org/10.5194/amt-2020-81
Preprint. Discussion started: 15 April 2020

Atmospheric Measurement Techniques Discussions

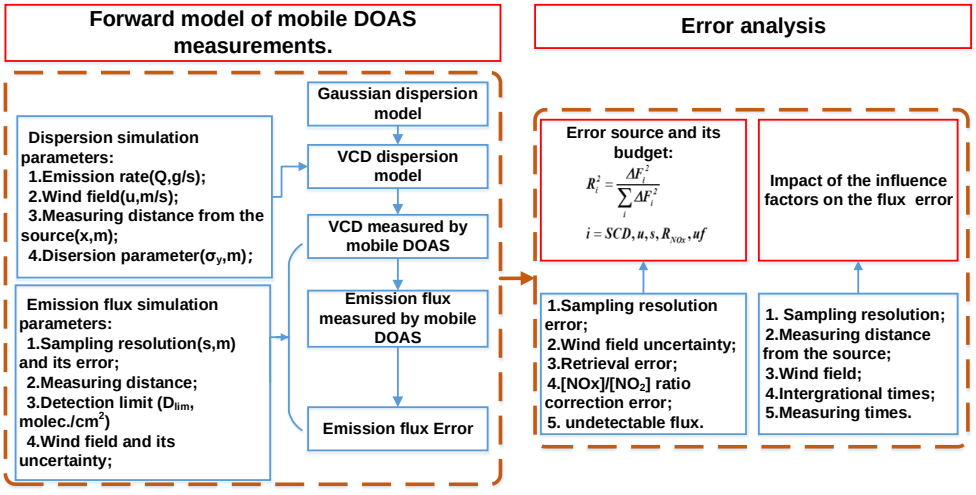

Figure 2. Forward model of mobile DOAS measurements and error analysis

The forward model of mobile DOAS measurements can be divided into 2 steps:

(1) Dispersion simulation. In this step, a dispersion model is established to generate the vertical column densities (VCDs) measured by the mobile DOAS in the modeled typical measurement.

(2) Emission flux simulation. After the VCD sequence along the measurement route is generated, the next step is calculating the emission flux and the emission flux error.

Error analysis:

This step concentrates on the error sources and their budget, and the influence factors that affect the emission flux error.

The emission flux and VCD retrieval calculation model can be directly introduced into our forward model, as it has in previous studies. However, some questions concerning the forward model still exist:

(1) Is the existing dispersion model suitable for the mobile DOAS measurement depicted in Figure 1?

(2) How can VCDs be simulated in the same way as mobile DOAS measurements in theory?

(3) Mobile DOAS can measure NO_2 instead of NOx. How can the $NO \leftrightarrow NO_2$ conversion be added to the existing dispersion model in terms of this simulation?

These questions will be explored in Sections 2.2–2.6.

https://doi.org/10.5194/amt-2020-81
Preprint. Discussion started: 15 April 2020

Atmospheric Measurement Techniques Discussions

2.2 Description of Gaussian dispersion model

2.2.1 Steady-state Gaussian dispersion model

An appropriate air dispersion model needed to be chosen for generating the forward model of mobile DOAS measurements. Since the concentrations of pollutants at individual points in the plume can be calculated based on the Gaussian dispersion model (Arystanbekova et al., 2004; Lushi et al., 2010; de Visscher, 2014), we applied the Gaussian dispersion model in this study. The plume, as reflected by the surface due to the ground boundary effect and the dispersion model, can be expressed as Eq. (1).

$$c(x,y,z)=\frac{DQ}{2\pi u\sigma_y\sigma_z}\exp(-\frac{y^2}{2\sigma_y^2})\cdot\{\exp[-\frac{(z+H)^2}{2\sigma_z^2}]+\exp[-\frac{(z-H)^2}{2\sigma_z^2}]\} \quad (1)$$

where Q is the emission rate (g/s); u is the wind speed (m/s) and the wind direction is along the *x*-direction; σ_y (m) is the dispersion parameter in the *y*-direction; σ_z (m) is the dispersion parameter in the *z*-direction, with σ_y and σ_z dependent on *x*; and H is the plume height (m). $D=\exp(-\varphi\frac{x}{u})$ is the decay term, mainly consisting of the chemical reactions and deposits; φ is the decay coefficient; and $\varphi=\frac{\ln 2}{T_{1/2}}$, in which $T_{1/2}$ is the pollutant half-life in seconds.

The dispersion parameters are determined by the atmospheric stability. The classification of atmospheric stability, which was created by Pasquill and Gifford and is widely used, sorts atmospheric stability into 6 classes ranging from A–F (de Visscher, 2014). We only considered the classifications under strong solar radiation (see Table 1) in this study.

Table 1. Pasquill–Gifford atmospheric stability classifications:

Wind Speed at 10m above the surface (m/s)	Strong Solar Radiation class
<2	A
2~3	between A and B
3~5	B
5~6	C
>6	C

A: very unstable; B: moderately unstable; C: slightly unstable

Based on the atmospheric stability class and the terrain type surrounding the emission point, the parameters σ_y and σ_z can be calculated. Since we assumed the surrounding area to be

https://doi.org/10.5194/amt-2020-81
Preprint. Discussion started: 15 April 2020

Atmospheric Measurement Techniques Discussions

flat, rural terrain, the σ_y and σ_z parameters could be calculated using Briggs's (1973) formulas, listed in Table 2

Table 2. Rural area air dispersion parameters (Briggs, 1973)

Stable classes	$\sigma_y(x)$	$\sigma_z(x)$
A	$0.22x(1+0.0001x)^{-0.5}$	$0.2x$
B	$0.16x(1+0.0001x)^{-0.5}$	$0.12x$
C	$0.11x(1+0.0001x)^{-0.5}$	$0.08x(1+0.0002x)^{-0.5}$
D	$0.08x(1+0.0001x)^{-0.5}$	$0.06x(1+0.0015x)^{-0.5}$
E	$0.06x(1+0.0001x)^{-0.5}$	$0.03x(1+0.0003x)^{-1}$
F	$0.04x(1+0.0001x)^{-0.5}$	$0.016x(1+0.0003x)^{-1}$

in which x is the horizontal distance from the source, m.

Since the wind field varies with time in actual measurements, the y-direction dispersion parameter needs to be adjusted using Eqs. (2) and (3), while z for the plume height does not, as we assume it to be higher than 200 m (de Visscher, 2014).

$$\sigma_{y2} = \sigma_{y1}\left(\frac{t_2}{t_1}\right)^p \tag{2}$$

$$\sigma_{y3} = \sqrt{\sigma_{y2}^2 + 0.1\Delta h^2} \tag{3}$$

where σ_{y1} (regarded as the Table 2 value) and σ_{y2} are the dispersion parameters obtained with averaging times of t_1 and t_2, respectively, with t_1 set to 10 min and t_2 to 60 min; σ_{y3} is the final dispersion parameter after correction. p is an empirical value of approximately 0.2 and Δh is the plume rise.

It should be noted that Briggs's equations are only suitable under the condition of x lower than 10 km. In addition, the model accuracy significantly decreases in the case of wind speeds either < 1.2 m/s or too strong (de Visscher, 2014). The upper wind speed has not been specified, so we set it to be 8 m/s.

https://doi.org/10.5194/amt-2020-81
Preprint. Discussion started: 15 April 2020


Atmospheric Measurement Techniques Discussions

2.2.2 NOx dispersion

Eq. (1) is suitable for SO_2 dispersion, while for NOx, mobile DOAS can only measure NO_2 effectively. Hence, Eq. (1) should be adjusted for NO_2 dispersion based on NOx atmospheric chemical reactions. In this study, we did not take Volatile Organic Compounds (VOCs) into consideration; thus, a NOx balance would not be broken. The typical reactions of NO, NO_2, O_3, and O_2 are:

$$NO_2 + h\nu \rightarrow NO + O(^3P) \quad \text{(reaction 1)}$$

$$O_2 + O(^3P) \rightarrow O_3 \quad \text{(reaction 2)}$$

$$NO + O_3 \rightarrow NO_2 + O_2 \quad \text{(reaction 3)}$$

The reaction rates of reactions 1, 2 and 3 form a cyclic reaction. The reaction rate of NO_2 is:

$$r_{NO2} = -j_3[NO_2] + k_5[NO][O_3]_t \quad (4)$$

where [gas] stands for the concentration of a particular gas; $[O_3]_t$ is the O_3 mean concentration in the plume at time t; t is the time period after NOx is emitted into the atmosphere; j_3 is the NO_2 photochemical rate constant, equal to approximately $8\times10^{-3}\ s^{-1}$; and k_5 is the rate constant of reaction 3, equal to approximately $1.8\times10^{-14}\ cm^3 molecules^{-1} s^{-1}$. It should be noted that these rates are for a temperature of 25°C. Fortunately, they are not sensitive to temperature, so temperature sensitivity did not need to be considered.

The [NOx]/[NO_2] ratio depends on the mixing ratio of O_3. We assumed that at the beginning there is no O_3 in the air parcel of the plume. During the mixing with outside air, the O_3 concentration within the air parcel increases. For simplicity, we assumed that the O_3 concentration within the air parcel of the plume is the same everywhere. The mixing ratio of O_3 within the air parcel of the plume can then be estimated as:

$$[O_3]_t = [O_3]\frac{V_t - V_0}{V_t} = [O_3]\frac{S_t\Delta t - S_0\Delta t}{S_t\Delta t} = [O_3](1 - \frac{S_0}{S_t}) \quad (5)$$

where V_0 is the initial gas volume of the plume and S_0 is the initial gas cross-section of the

https://doi.org/10.5194/amt-2020-81
Preprint. Discussion started: 15 April 2020


Atmospheric Measurement Techniques Discussions

plume; while V_t is the gas volume of the plume at time *t* and S_t is the gas cross-section of the plume in the atmosphere at time *t*. Here, [O3] is the ambient O3 concentration. The NO2 concentration at time *t* is given by:

$$[NO_2]_t = \int_0^t r_{NO2} dt \tag{6}$$

Since the NO2 initial concentration was very low, we assumed the NO2 initial concentration $[NO_2]_0 = 0$. Consequently, $[NOx]_t = [NO]_0$ (with no decay).

The [NOx]/[NO2] ratio at time *t* is:

$$R_{NOx} = \frac{[NOx]_t}{[NO_2]_t} \tag{7}$$

Different from SO2, the number of NOx molecules is conserved, as opposed to their mass. The NOx dispersion model should thus be expressed as:

$$c_{NOx}(x,y,z) = \frac{DQ_{mNOx}}{2\pi u\sigma_y\sigma_z}\exp(-\frac{y^2}{2\sigma_y^2})\cdot\{\exp[-\frac{(z+H)^2}{2\sigma_z^2}]+\exp[-\frac{(z-H)^2}{2\sigma_z^2}]\} \tag{8}$$

where $Q_{mNOx} = \frac{Q\cdot NA}{m_{NOx}}$. m_{NOx} is the mean molar mass of the initial NOx and NA is Avogadro's constant of 6.02×10^{23} molecules mol^{-1}. Substituting Eq. (7) into Eq. (8), the NO2 dispersion model can then be expressed as:

$$c_{NO2}(x,y,z) = \frac{c_{NOx}(x,y,z)}{R_{NOx}} \tag{9}$$

2.3 VCD dispersion model

As discussed above, mobile DOAS retrieves the VCD, while results of the dispersion model are point concentrations. Based on the definition of VCD, we integrate the concentration along the vertical direction, i.e., the *z*-direction from the ground to the upper troposphere, as in:

$$\begin{aligned} VCD(x,y) &= \int_0^{+\infty} Dc(x,y,z)dz = \frac{DQ}{\sqrt{2\pi}u\sigma_y\sigma_z}\int_0^{+\infty}\{\exp[-\frac{(z+H)^2}{2\sigma_z^2}]+\exp[-\frac{(z-H)^2}{2\sigma_z^2}]\}dz \\ &= \frac{DQ}{\sqrt{2\pi}u\sigma_y}\exp(-\frac{y^2}{2\sigma_y^2}) \end{aligned} \tag{10}$$

https://doi.org/10.5194/amt-2020-81
Preprint. Discussion started: 15 April 2020

Atmospheric Measurement Techniques Discussions

Eq. (10) is suitable for SO_2. For NOx, the VCD dispersion is

$$VCD_{NOx}(x,y) = \frac{DQ_{mNOx}}{\sqrt{2\pi}u\sigma_y}\exp(-\frac{y^2}{2\sigma_y^2}) \tag{11}$$

The NO_2 VCD dispersion model is

$$VCD_{NO2}(x,y) = \frac{VCD_{NOx}(x,y)}{R_{NOx}} \tag{12}$$

Eqs. (10), (11), and (12) lay the mathematical foundation of the VCD distribution model for mobile DOAS measuring.

2.4 VCD measured by mobile DOAS

As shown in Figure 3, the flux of the plume cross-section can be calculated using the following equation:

$$\Delta F = u \cdot \int_l VCD(x,y)ds \tag{13}$$

For actual measurements, ΔF should be given by Eq. (14)

$$\Delta F = VCD_j \cdot u \cdot s \tag{14}$$

where s is the distance between 2 measuring points and VCD_j can be derived from the spectrum of measurement j. Based on Eqs. (13) and (14), VCD_j can be expressed by Eq. (15)

$$VCD_j = \frac{1}{s}\int_l VCD(x,y)ds \tag{15}$$

Eq. (15) indicates that the VCD_j derived from individual mobile DOAS measurements is the average of $VCD(x,y)$ along the measurement route. The discretization of the VCD can significantly affect the emission flux error and will be discussed in Section 4.1.

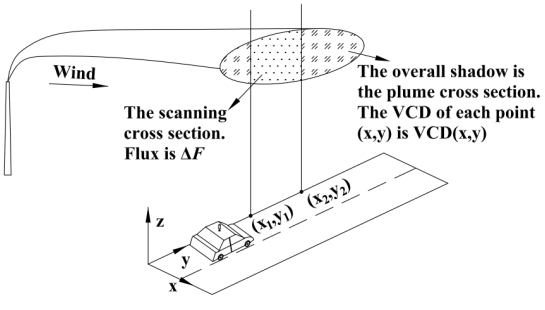

Figure 3. Model of VCD measured by mobile DOAS

https://doi.org/10.5194/amt-2020-81
Preprint. Discussion started: 15 April 2020

Atmospheric Measurement Techniques Discussions

2.5 Description of emission flux measured by mobile DOAS

The equation for calculating emission flux in the discrete form is expressed as

$$F = \sum_i VCD_i \cdot \vec{u_i} \cdot \vec{n}_i \cdot s_i \tag{16}$$

where F is the emission flux; VCD_i is the VCD for DOAS measurement i along the measurement route; $\vec{u}_i$ is the wind field; $\vec{n}_i$ is the vector pointing to the right of the driving direction and parallel to the Earth's surface; and s_i is the sampling resolution. Since the SO_2 lifetime scale is longer than the dispersion time scale, a decay correction is not needed for SO_2, but for NOx it can be necessary.

The NOx emission flux is then:

$$F_{NOx} = \frac{R_{NOx}}{D} F_{NO2} \tag{17}$$

In fact, the decay correction for NOx should be applied for cases with low wind speeds, while the effect for high wind speeds is very small.

2.6 Measurement errors of emission flux

The emission flux measurement errors by mobile DOAS have several sources: SCD retrieval errors, AMF errors, wind field uncertainties, sampling resolution error, and undetectable flux. The undetectable flux is attributed to the ambient SCD below the mobile DOAS detection limit, which results in undetectable SCDs as well as undetectable flux. The total relative error of the emission flux is given by:

$$E_{total} = \frac{F_{err}}{D \cdot Q} = \frac{\sqrt{\Delta F_{uf}^2 + \Delta F_{VCD}^2 + \Delta F_{\vec{u}}^2 + \Delta F_s^2}}{D \cdot Q} \times 100\% \tag{18}$$

where F_{err} is the flux error, and ΔF_{VCD} is the flux error introduced by VCD error, which mainly arises from the SCD retrieval error and the AMF error. For the low plume heights and small amounts of aerosols within the plume in this study, the SCD could always be assumed to be equal to the VCD. The AMF error is thus negligible. ΔF_{uf} is the undetectable flux; $\Delta F_{\vec{u}}$ is the flux error introduced by wind speed uncertainty and wind direction uncertainty, i.e., the wind field uncertainty; and ΔF_s is the emission flux error introduced by sampling resolution

https://doi.org/10.5194/amt-2020-81
Preprint. Discussion started: 15 April 2020


Atmospheric Measurement Techniques Discussions

measuring error.

Eq. (18) is appropriate for SO_2. With regard to NOx, the NOx flux error is also introduced by the decay correction and the [NOx]/[NO_2] ratio correction error. Hence, the NOx flux relative error is:

$$E_{NOx} = \frac{F_{err}}{D \cdot Q} = \frac{\sqrt{\Delta F_D^2 + \Delta F_{R_{NOx}}^2 + \Delta F_{uf}^2 + \Delta F_{VCD}^2 + \Delta F_{\bar{u}}^2 + \Delta F_s^2}}{D \cdot Q} \times 100\% \quad (19)$$

where ΔF_D is the flux error due to decay correction, and ΔF_{RNOx} is the flux error due to [NOx]/[NO_2] ratio correction.

In order to quantify the contributions/budget of individual error sources, the ratios are calculated as Eq. (20)

$$R_i^2 = \frac{\Delta F_i^2}{F_{err}^2} \quad (20)$$

where i represents the individual error sources. Note that $\sum_i R_i^2 = 1$.

3 Parameter assumption and numerical simulation

In Section 2, the forward model for mobile DOAS measurements of emission flux was established. In this section, reasonable values of the parameters in the forward model are discussed and prepared in order to drive the forward model.

For most factories, including power plants, the emission rates of NOx and SO_2 are different. Since a higher emission rate is an ideal condition for mobile DOAS measurements, higher emissions could be outside the scope of our study. Therefore, the emission rate that we simulated was < 200 g/s, and we set the Q value within this range. Since the Gaussian dispersion model is appropriate for moderate wind speed and scale, the wind speed was set to range from 1.2–8 m/s and the dispersion distance was approximately 0–10 km. Given the car speed and mobile DOAS spectrometer integration times t_{int}, the sampling resolution was set from 5–500 m. The NOx mean daytime lifetime is approximately 5 h $\pm$ 1 h (Spicer, 1982), while the SO_2 daytime lifetime is more than 1 day (S. Beirle, 2014). Compared with the dispersion time scale, the SO_2

https://doi.org/10.5194/amt-2020-81
Preprint. Discussion started: 15 April 2020

Atmospheric Measurement Techniques Discussions

daytime lifetime uncertainty could be neglected. When time approaches infinity, the NOx reaction steady-state could be determined by ambient [O_3] according to Eq. (4). We here assumed a typical [O_3] value 1.389×10^{12} molec. /cm^3 thus the steady-state [NOx]/[NO_2] ratio is 1.32. The [NOx]/[NO_2] ratio inside the air parcel of the plume varying with the distance could be determined by Eqs. (4), (5), (6) and (7).

The VCD error can mainly be attributed to the DOAS fit error of the SCD. Previous studies have indicated that the typical errors of NO_2 and SO_2 VCDs are ~2.5×10^{15} molecules cm^{-2} and ~4×10^{15} molecules cm^{-2}, respectively. The sampling resolution error is primarily attributed to the drift of GPS and but it is negligible in actual measurements due to individual GPS errors cancel each other.

The wind field uncertainty includes both wind direction uncertainty and wind speed uncertainty. In order to quantify the 2 uncertainties, the 1-month wind profile data at the height of 250 m during the time period 9:00–16:00 from 1 April–30 April 2019 were derived from the Doppler wind profile radar located in Shijiazhuang (38.17ºN, 114.36ºE). The average wind fields and standard deviations were calculated for each hour, as shown in Figure 4. Two-order polynomials were applied in order to derive the function of standard deviation versus average value for both wind speed and wind direction. Some sample values calculated using these polynomials are listed in Table 3. Table 4 lists all the simulation parameters of NOx and SO_2 that were required.

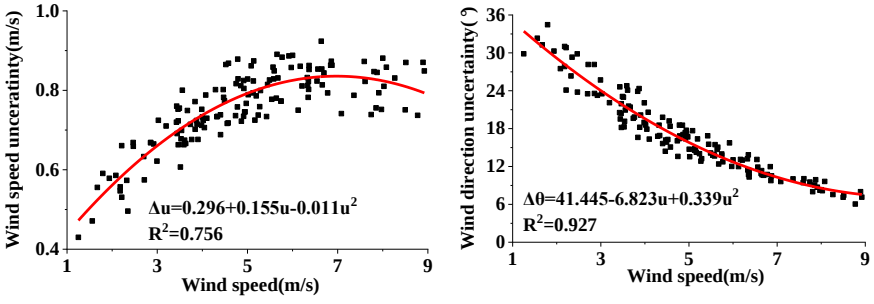

Figure 4. Polynomial fitting of the uncertainty between wind speed and wind direction

Table 3. Wind speed uncertainty and wind direction uncertainty after polynomial fitting

wind speed(m/s)	wind speed uncertainty(±,m/s)	wind direction uncertainty(±,°)
1.2	0.46616	33.74556

https://doi.org/10.5194/amt-2020-81
Preprint. Discussion started: 15 April 2020

2	0.562	29.155
3	0.662	24.027
4	0.74	19.577
5	0.796	15.805
6	0.83	12.711
7	0.842	10.295
8	0.832	8.557

Table 4. Simulation parameters and data range of NOx and SO_2

Parameter	Values
Emission rate(g/s)	10, 30, 50, 100 , 150, 200
Wind speed(m/s)	1.2, 2,3, 4, 5, 6, 7, 8
Measuring distance(km)	0~10km
Sampling resolution and its error(m)	5~500m, initial integration times t_{int}
Retrieval error(molec.cm^{-2})	NO_2: ~2.5×10^{15}; SO_2: ~4×10^{15}
Detection limit(molec.cm^{-2})	NO_2:5×10^{15}; SO_2:8×10^{15}
Average atmosphere lifetime	NOx:5h±1h; SO_2: more than 1 day
R_{NOx}	R_{NOx} inside the plume is calculated by Eqs. (4), (5), (6) and (7). R_{NOx} in steady-state is 1.32.

The parameters listed in Table 4 were applied in the forward model in order to perform the simulation. The simulation results are shown in Figures 23 and 24 of the Appendix.

4 Analysis of emission flux errors measured by mobile DOAS based on the forward model

Figures 23 and 24 in the Appendix show that the modeled relative errors of NOx and SO_2 emission flux varied with sampling resolution and distance from the point source under different wind speeds and emission rates. Some overall features can be derived from these figures. Therefore, typical cases were selected in order to discuss the overall features based on several key factors.

4.1 Sampling resolution and its error

Sampling resolution variation impacts on the error combination and propagation and its measuring error is an error source.

The typical uncertainty of the GPS readings is <1.5m. For measurements with small sampling

https://doi.org/10.5194/amt-2020-81
Preprint. Discussion started: 15 April 2020

Atmospheric Measurement Techniques Discussions

resolutions the GPS error can thus cause relatively large uncertainties for the flux contributions from individual measurements (Eq. 14). However, even for small sampling resolutions the GPS errors of neighboring flux contributions almost completely cancel each other. Thus the contribution of the GPS error to the flux calculation (Eq. 16) can be neglected.

In order to discuss the dependence of flux error on sampling resolution, some data were extracted from the Appendix and plotted in Figure 5. This figure shows the increase of relative error with increasing sampling resolution. It should be noted that the smaller the sampling resolution, the more data the mobile DOAS will sample. This directly leads to the inclusion of more data in the emission flux calculations, resulting in the lower emission flux error. However, when far from the source, the plume with narrows quickly (see section 4.2). Appling different sampling resolution is no longer feasible. Therefore, the sampling resolution can only work effectively when the measurements are not far from the source.

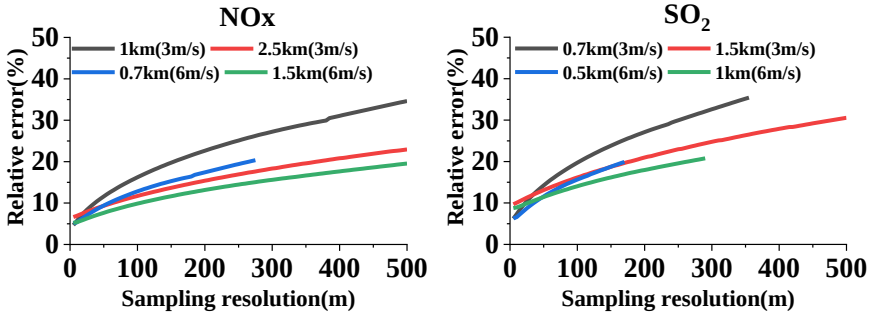

Figure 5. Dependence of relative errors on sampling resolution (Q = 100 g/s, u = 3 m/s and 6 m/s, at different measuring distances)

The impact of sampling resolution on emission flux error is noticeable. In terms measurement efficiency, the sampling resolution should be moderate. Therefore, we recommend the proper sampling resolution to be between 5 m and 50 m. Larger resolutions may also be viable, but > 100 m is not recommended.

4.2 Measuring distance from the source

Measuring distance is not an error source, but affects the dispersion and NOx chemical reactions, further adding to the emission flux error. Figure 6 presents typical examples of relative errors varying with distance at a resolution of 20 m. Wind speeds of 3 m/s and 6 m/s were

https://doi.org/10.5194/amt-2020-81
Preprint. Discussion started: 15 April 2020

Atmospheric Measurement Techniques Discussions

utilized in this example. The overall feature shown in all of the sub-figures of Figure 6 is the rapid decrease and then quick increase of the relative error with measuring distance. Different factors lead to the large errors at small and large distances.

First, we analyzed NOx and SO_2 emission flux errors for a large measuring distance. The large distance results in the dramatic decrease of ambient VCDs due to dispersion and decay along the plume transport path. The ambient VCDs can be lower than the detection limit of mobile DOAS measurements, resulting in a portion of the undetectable flux. Because of dispersion, the plume widths with VCDs above the detection limit and thus the detectable fluxes decrease significantly with distance, even dropping to 0, as shown in Figure 6. This causes the relative error to increase at large measuring distances.

Second, we analyzed NOx and SO_2 emission flux errors in the case of a small measuring distance. Figure 6 indicates that the error is large and decreases rapidly with increasing measuring distance when close to the source. As discussed in Section 4.1, if more measurement data are included in the calculations of flux, the relative error can decrease. When the measuring distance is small, the number of samples can dramatically decrease. For SO_2, the relative error can increase significantly when the measurements are close to the point source. For NOx, the relative error is also affected by chemical reactions, this phenomenon that we will discuss in Section 4.4.

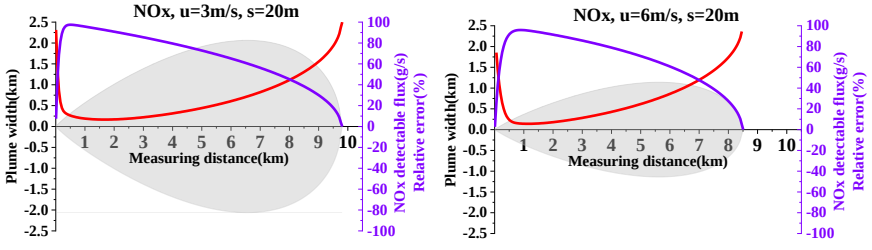

https://doi.org/10.5194/amt-2020-81
Preprint. Discussion started: 15 April 2020

Atmospheric Measurement Techniques Discussions

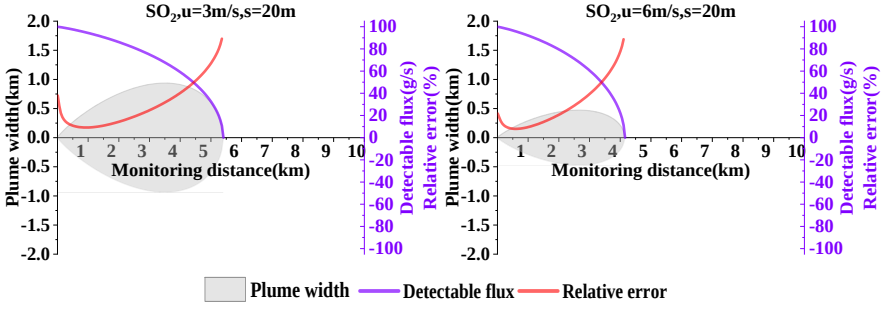

Figure 6. Variation of NOx and SO_2 relative errors with distance, using Eqs. (18) and (19) (Q = 100 g/s, setting the sampling resolution *s* = 20 m and the wind speed to 3 m/s and 6 m/s)

4.3 Wind fields and their uncertainty

Wind fields can impact both the gas dispersion (Eqs. 1, 8, 9) and the calculation of emission flux (Eqs. 16, 17). In terms of dispersion, wind speed affects gas VCD (Eqs. 10, 11, 12). In terms of flux calculation, the temporal and spatial uncertainty of wind fields can contribute to emission flux calculation errors. Therefore, the effects of wind fields are discussed based on these 2 factors in this section.

Figure 7 displays the variations of the relative errors of NOx and SO_2 with wind speed at different distances. The emission rate Q and the sampling resolution are chosen as 100 g/s and 20 m, respectively. Figure 7 indicates the different features of relative error for wind speeds at small and large measurement distances. The relative error of NOx increases with increasing wind speed at different distances, while the SO_2 relative error for measurements at small distances exhibits a trend opposite that of the large distance measurements. The causes of the different relationships at small and large measurement distances are discussed in subsection 4.3.1.

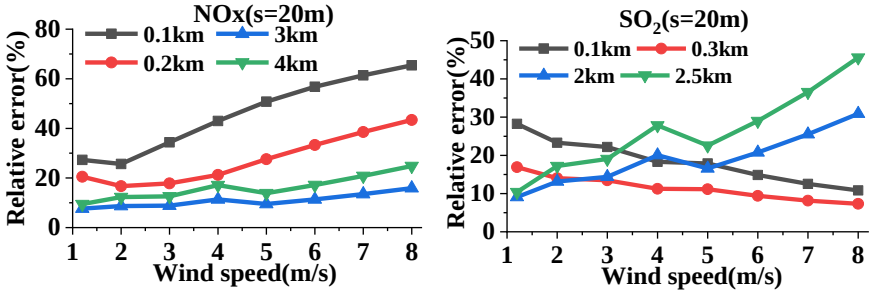

https://doi.org/10.5194/amt-2020-81
Preprint. Discussion started: 15 April 2020


Atmospheric Measurement Techniques Discussions

399 Figure 7. Relative errors of NOx and SO_2 emission flux changes with wind speed at different measure-
400 ment distances (Q = 100 g/s, sampling resolution s = 20 m)
401
402 **4.3.1 Effects of different wind speeds on measurements at small and large measurement**
403 **distances**
404 Since the NOx and SO_2 flux measurement errors of different wind speeds are very different
405 at small and large measurement distances, we discuss them separately.
406 **4.3.1.1 SO_2**
407 We first analyzed the effect of different wind speeds on the SO_2 emission flux error.
408 Since VCDs decrease with increasing wind speed (Eqs. 10, 11, 12), more ambient VCDs
409 would be below the detection limit of mobile DOAS at high wind speeds. Hence, the contribu-
410 tion of undetectable ambient VCDs to the error of flux calculations depends on wind speed. In
411 addition, since wind fields are input into the calculations of emission flux (Eqs. 16, 17), their
412 uncertainties can contribute to the flux measurement error. In order to investigate the contribu-
413 tions of undetectable ambient VCDs and the influence of wind field uncertainties in flux meas-
414 urement, the ratios R_{uf}^2 (R^2 of the undetectable flux) and R_u^2 (R^2 of the wind field uncertainty)
415 calculated using Eq. (20) are shown in Figures 8c and 8d for different wind speeds and meas-
416 urement distances.
417 Again, we first analyzed the measurements at large distances, finding that R_{uf}^2 is greater
418 than R_u^2 for large measurement distances, as shown in Figures 8c and 8d. Therefore, undetect-
419 able VCDs dominate the effect of wind fields on the error of flux calculations when the meas-
420 urement distance is large. Since VCDs decrease with increasing wind speeds, the flux error
421 associated with undetectable VCDs should be increased with wind speed. This relationship ex-
422 plains the phenomenon that the relative error of emission flux increases with increasing wind
423 speed for large measurement distances.
424 Next, the measurements at small distances were analyzed. Figures 8c and 8d indicate that

https://doi.org/10.5194/amt-2020-81
Preprint. Discussion started: 15 April 2020

Atmospheric Measurement Techniques Discussions

425 R_{uf}^2 is much lower than R_u^2 for short measurement distances. The wind field uncertainty dom-
426 inates the effect of wind fields on the flux calculation errors. Meanwhile, since the relative
427 uncertainty of the wind field decreases with increasing wind speed, the emission flux error
428 decreases with increasing wind speed for short measurement distances, as shown in Figure 6.

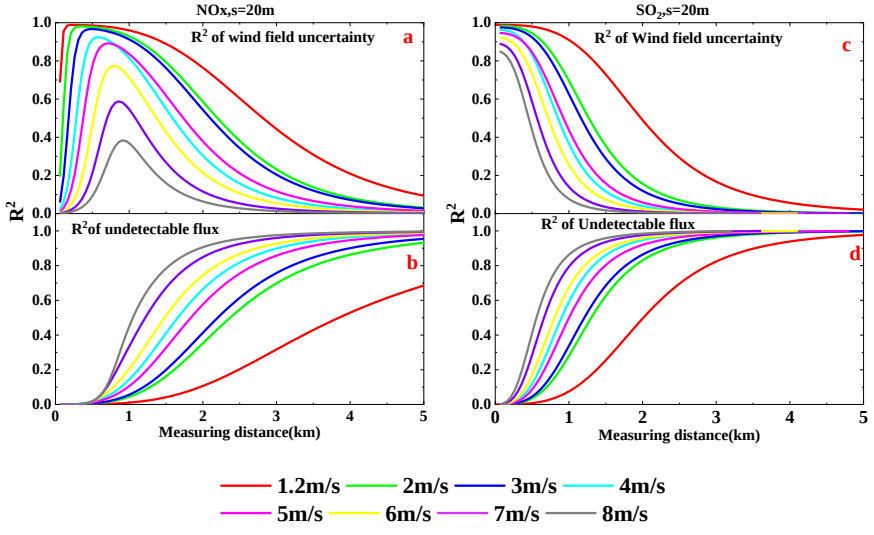

429
430

431 Figure 8. Wind field uncertainty ratio squared R_u^2 and undetectable emission flux ratio squared R_{uf}^2 of
432 NO_2 and SO_2 emission flux measurement error changes with measurement distance for different wind
433 speeds (Q = 100 g/s, sampling resolution s = 20m)
434

435 **4.3.1.2 NOx**

436 We next analyzed the effect of different wind speeds on NOx emission flux error, as shown
437 in Figures 9a and 9b.

438 The effects of different wind speed dispersions on NOx emission flux error are similar to
439 SO_2, i.e., Figures 9b and 9d, indicating that the effects of wind speed dispersion are analogous.
440 The effect of wind field uncertainty is much different from SO_2, however, especially when the
441 measurements are very close to the source. When very close, wind field uncertainty influence
442 increases and then decreases with distance. Compared with SO_2, the decreasing trend of NOx
443 in the case of far measurement distances is also similar, but the increasing trend is very different.
444 This implies that NOx measurements close to the source have another main potential error

https://doi.org/10.5194/amt-2020-81
Preprint. Discussion started: 15 April 2020


Atmospheric Measurement Techniques Discussions

source, which we will investigate in Section 4.4.

The 4 subfigures in Figure 9 share the common characteristic that the R^2 lines have intersections between 4 m/s and 5 m/s. This implies that the wind field uncertainty effect and the wind field dispersion effect are distinguished between 4 m/s and 5 m/s. In actual measurements, undetectable VCDs cannot be well quantified. Therefore, we recommend the proper wind speed for mobile DOAS to be < 4 m/s. The appropriate lower wind speed in this study was 1.2 m/s, But the Gaussian plume model we used becomes increasingly inaccurate when wind speeds are under 1m/s. Thus, we recommend a proper wind speed of 1–4 m/s.

4.3.2 Error budget of undetectable flux, uncertainties of wind direction and speed

The remaining question is what flux error budget is associated with the wind field. From Section 2.6 we know that R_u^2 (R^2 of wind speed uncertainty) and R_{Dir}^2 (R^2 of wind direction uncertainty) constitute R_u^2. The R_{uf}^2 value of the undetectable flux is the contribution of the wind field dispersion. Figure 9 presents the changes of R_u^2, R_{Dir}^2, and R_{uf}^2 of NOx and SO_2 with distance for different wind speeds, 3 m/s and 6 m/s.

As for SO_2, the wind field influence contributes most of the emission flux error from wind field uncertainty, in conjunction with wind dispersion. From Figure 9, we can infer that the sum of R_u^2, R_{Dir}^2, and R_{uf}^2 is > 0.9. Furthermore, contributions from wind speed uncertainty and wind direction uncertainty in the emission flux error are also presented in Figure 9. This demonstrates that wind direction uncertainty contributes about 0.78 to the wind field uncertainty when the wind speed is 3 m/s and 0.74 when the wind speed is 6 m/s.

With regard to NOx, the wind field influence is similar to SO_2 when measuring far from the source and very different when measuring close to the source. As discussed above, mobile DOAS can only measure the NO_2, as opposed to the NOx. The amount of NO_2 yield determines the mobile DOAS measurement result, and thus that of the NOx flux measurement error, especially when measuring very close to the source.

https://doi.org/10.5194/amt-2020-81
Preprint. Discussion started: 15 April 2020

Atmospheric Measurement Techniques Discussions

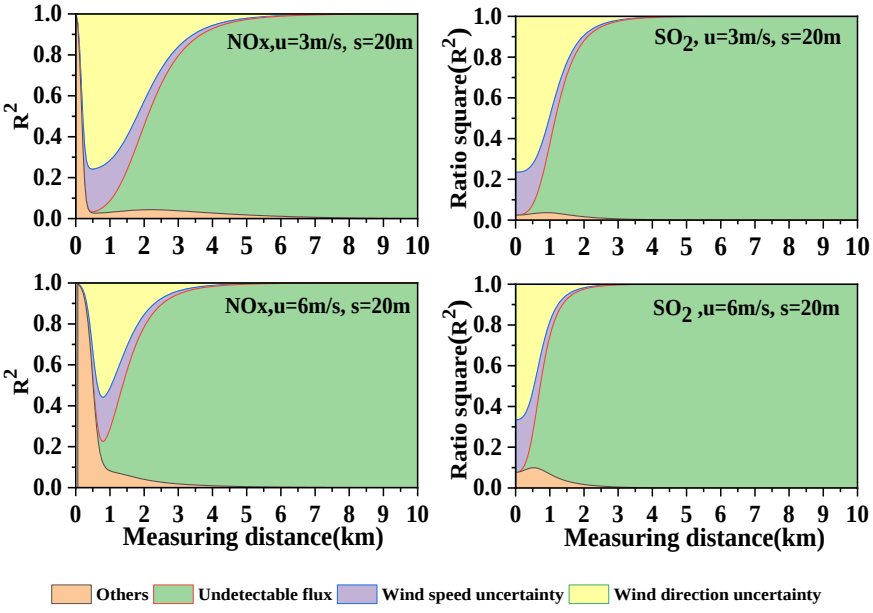

Figure 9. Changes of R_u^2, R_{Dir}^2, and R_{uf}^2 of NOx and SO_2 emission flux measurement errors with measurement distance for different wind speeds (Q = 100 g/s)

4.4 NOx chemical reactions

In Section 4.2 we left unanswered the question as to why the NOx flux error is very large when very close to the source (see Figure 6). In this section we will investigate the reason for this phenomenon.

Stacks mainly exhaust NO, which then transforms into NO_2 in a few minutes due to chemical reactions. Since NOx disperses along the wind direction, this means that the $[NO_2]/[NOx]$ ratio varies with distance. We calculated the $[NO_2]/[NOx]$ ratio and displayed it in a subfigure of Figure 10. From Figure 10a we can see that the $[NO_2]/[NOx]$ ratio increases with distance.

In actual measurements, especially for elevated point sources, the dependence of the $[NOx]/[NO_2]$ ratio on the distance from the air parcel of the plume is difficult to measure. Thus for the NOx flux calculations, a $[NOx]/[NO_2]$ ratio correction factor is applied. However, since the assumptions for the calculation of this correction factor might be different from the true conditions, even after the application of the correction factor, substantial flux errors might occur. Subfigure b in Figure 10 displays the R_{RNOx}^2 value of the $[NOx]/[NO_2]$ ratio correction error.

https://doi.org/10.5194/amt-2020-81
Preprint. Discussion started: 15 April 2020

Atmospheric Measurement Techniques Discussions

The larger the [NOx]/[NO2] ratio, the larger the R^2_{RNOx} value of the [NOx]/[NO2] ratio correction. This causes the R^2_{RNOx} to increase, to as high as 1, when near the source. Also, from the R^2_{RNOx} value we discovered that the [NOx]/[NO2] ratio correction error is the main error source when close to the emission source. Hence, the main flux error source near the emission source is the [NOx]/[NO2] ratio correction error.

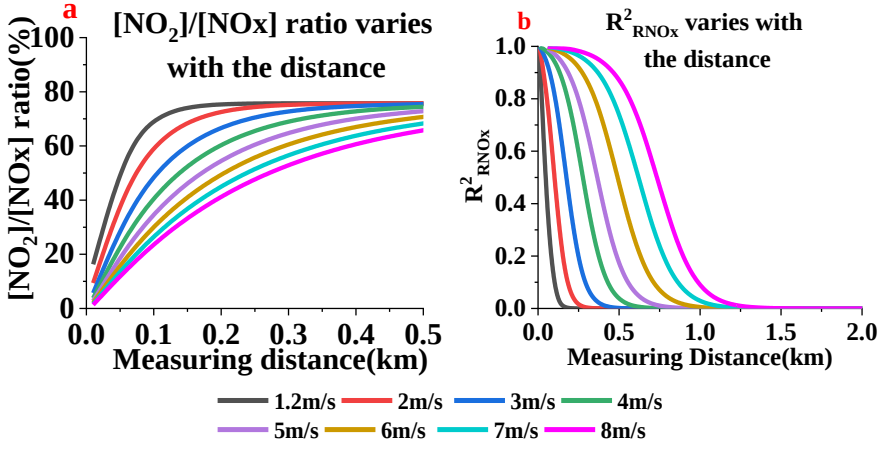

Figure 10. Variation of [NO2]/[NOx] ratio and R^2_{RNOx} with distance at different wind speeds (Q = 100 g/s)

Since we know that the [NOx]/[NO2] ratio correction error is the main error source near the emission source, developing ways to avoid or minimize this error is our goal.

In real-world experiments, accurately measuring NOx flux requires NOx to reach a steady state. According to Eq. (4), when time approaches infinity, the NO2 reaction rate r_{NO2} approaches 0, indicating that NOx reaches a steady-state. In theory, steady-state NOx is an ideal condition for measuring NOx flux. Infinite time, however, is not our expectation. If we regard $r_{NO2} = 0.05 r_{\max}$ as the approached steady-state, the approached steady-state time could be attained, as well as the approached steady-state distance. $r_{\max}$ is defined as the theoretical NO2 maximal reaction rate, which is $r_{NO2} = k_5[NO]_0[O_3]$. Figure 11 a displays the variation of $\frac{r_{NO2}}{r_{\max}}$ with time and Figure 11 b displays the approached steady-state distance.

https://doi.org/10.5194/amt-2020-81
Preprint. Discussion started: 15 April 2020

Atmospheric Measurement Techniques Discussions

In order to investigate the feasibility of our recommendation, we used the following equation for analysis:

$$E_{RNOx} = \frac{\Delta F_{RNOx}}{DQ} \times 100\% \quad (21)$$

where ΔF_{RNOx} is the flux error resulting from the [NOx]/[NO_2] ratio correction at the approached steady-state distance. E_{RNOx} is used rather than R^2 because R^2 only represents the error source contribution/budget. For example, the R^2 value of the [NOx]/[NO_2] ratio correction is 0.9, while the total relative error is only 10%. In this case, it seems that we cannot accept the high R^2, although the total relative error is acceptable. Therefore, in our judgment, using E_{RNOx} is an advantage.

The E_{RNOx} values at the approached steady-state distance for different wind speeds and emission rates were calculated, and the results are presented in Figure 11 c. From this figure, we can infer that E_{RNOx} is approximately 5%, which is very low. This indicates that the flux error resulting from the [NOx]/[NO_2] ratio correction at the approached steady-state distance is very small and can thus be regarded as negligible.

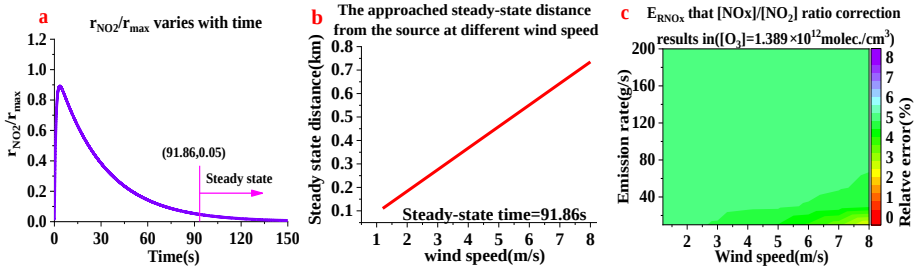

Figure 11. NOx steady-state distance from the source and the E_{RNOx} values under different emission rates and wind speeds ([O_3]= 1.389 × 10^{12} molecules/cm^3)

According to Eq. (6), r_{NO2} depends on [O_3]. Hence, we also calculated the NOx steady-state distance and E_{RNOx} under different [O_3]. The E_{RNOx} was also approximately 5% under different [O_3], as shown in Figure 12. The dependence calculation demonstrates that E_{RNOx} is also

https://doi.org/10.5194/amt-2020-81
Preprint. Discussion started: 15 April 2020

Atmospheric Measurement Techniques Discussions

very small under different [O_3]. Consequently, regarding $r_{NO2} = 0.05 r_{max}$ as the approached steady state seems to be acceptable.

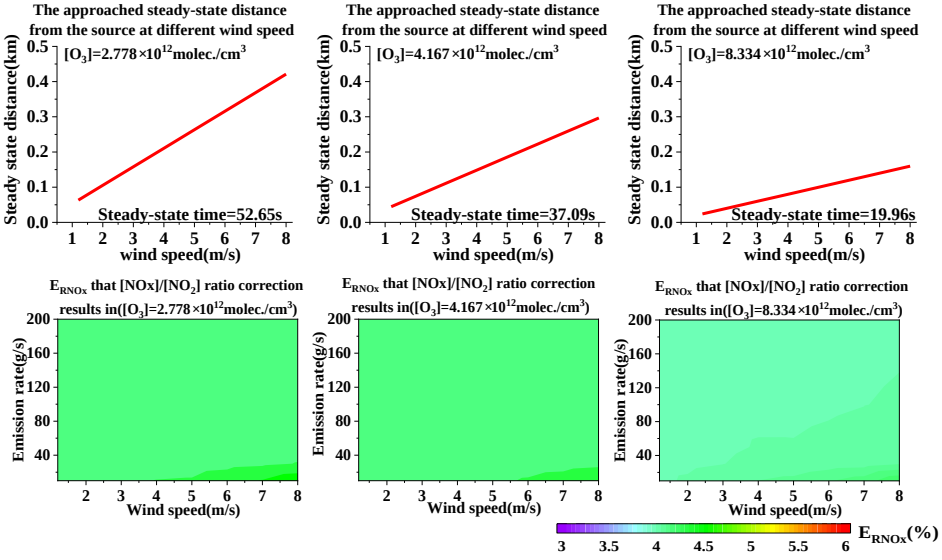

Figure 12. NOx approached steady-state distance from the source and E_{RNOx} values under different emission rates, different wind speeds, and different [O_3].

In summary, when very close to the emission source, the main flux error source is the [NOx]/[NO_2] ratio correction error. In order to avoid or minimize this error, we recommend $r_{NO2} = 0.05 r_{max}$ as the approached steady state, in which case the approached steady-state distance is the starting measurement distance. The overall distances for different [O_3] concentrations were also simulated as a reference for the DOAS measurement of NOx point source emissions, as shown in Figure 13. In subsection 2.2.2, we assumed that it was reasonable to disregard VOCs, since NOx, water vapor, and VOCs would generate a more complex reaction that could produce more O_3, which in turn would accelerate the NO_2 reaction rate. In other words, what we assumed is conservative, so the NOx approached steady-state distance in Figure 13 is also conservative.

https://doi.org/10.5194/amt-2020-81
Preprint. Discussion started: 15 April 2020

Atmospheric Measurement Techniques Discussions

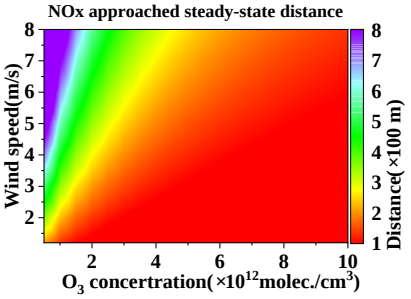

Figure 13. NOx steady-state distance from the source for different [O_3] concentrations ($r_{NO2} = 0.05 r_{max}$).

4.5 Retrieval error

Since the emission flux error due to the VCD retrieval error depends on the plume width and the sampling resolution, typical plume widths and sampling resolutions were selected for this discussion. We set the wind speeds at 1.2 m/s and 8 m/s because, based on the dispersion model, the plume width is a function of the wind speed (Eqs. 1, 8, 9). Sampling resolutions of 20 m and 100 m were chosen. In addition, an emission rate of 100 g/s for the point source Q was set. Figure 14 displays the total relative error, R^2_{VCD}, and the absolute flux error caused by the retrieval error. From this figure we could infer that the retrieval error is not the main error source for $R^2_{VCD} < 0.2$, although the R^2_{VCD} trend is very interesting.

R^2_{VCD} increases to a peak value and then decreases, while the absolute flux error slowly increases at relatively long range measurement distances and then quickly decreases. Meanwhile, the trend of total relative error quickly decreases (stage A in Figure 14) and then slowly increases (stage B in Figure 14). In order to simplify the analysis, we only designated stage A and stage B for the wind speed of 8 m/s. In stage A, the flux error grows while the total relative error decreases rapidly, resulting in the retrieval error contribution becoming more obvious. In stage B, the flux error slowly grows and then decreases, while the total relative error grows, resulting in the retrieval error contribution becoming less obvious. This results in the observed R^2_{VCD} trend.

https://doi.org/10.5194/amt-2020-81
Preprint. Discussion started: 15 April 2020

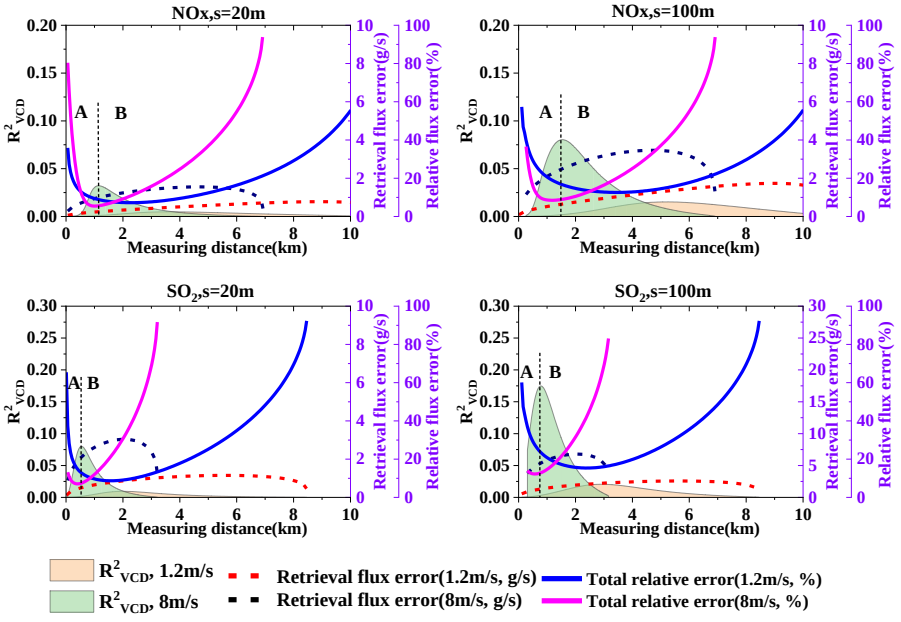

Figure 14. Total relative error, absolute flux error, and retrieval error resulting in the R^2_{VCD} trends of NO_2 and SO_2 (Q = 100 g/s)

4.6 Effect of number of measurement times

In our experiments, we only simulated a single scan of the plume by the mobile DOAS at each specific distance. In reality, we usually scan the plume cross-section several times in order to reduce the flux error. Figure 15 displays the simulation example of NOx and SO_2 flux error under different measurement times.

The error sources of the emission flux can be classified into 2 types. The first is the measurable error/uncertainty: wind speed and wind direction uncertainty, and retrieval error. The second is: [NOx]/[NO_2] ratio correction error near the source and undetectable flux error. The flux error resulting from the first type of error source can be lowered by scanning the plume more times while the second cannot be.

According to the analysis in Section 4.3, the undetectable flux is the main error source when far from the emission source. Consequently, the flux error under different numbers of scans for both NOx and SO_2 cannot be significantly lowered when measuring far from the source (range D in Figure 15). Within the close measurement range (range C in Figure 15), the first type of

https://doi.org/10.5194/amt-2020-81
Preprint. Discussion started: 15 April 2020

Atmospheric Measurement Techniques Discussions

error source is the predominant source of SO_2 error, and thus the flux error can be lowered by additional plume scans. For NOx, however, the [NOx]/[NO_2] ratio correction error is the main error source when very close to the emission source (range A in Figure 15), and thus the effect of additional plume scans is not evident. A little farther from the source, the first type of error source becomes the main error source (range B in Figure 15). Ultimately, the impact of additional plume scans becomes effective.

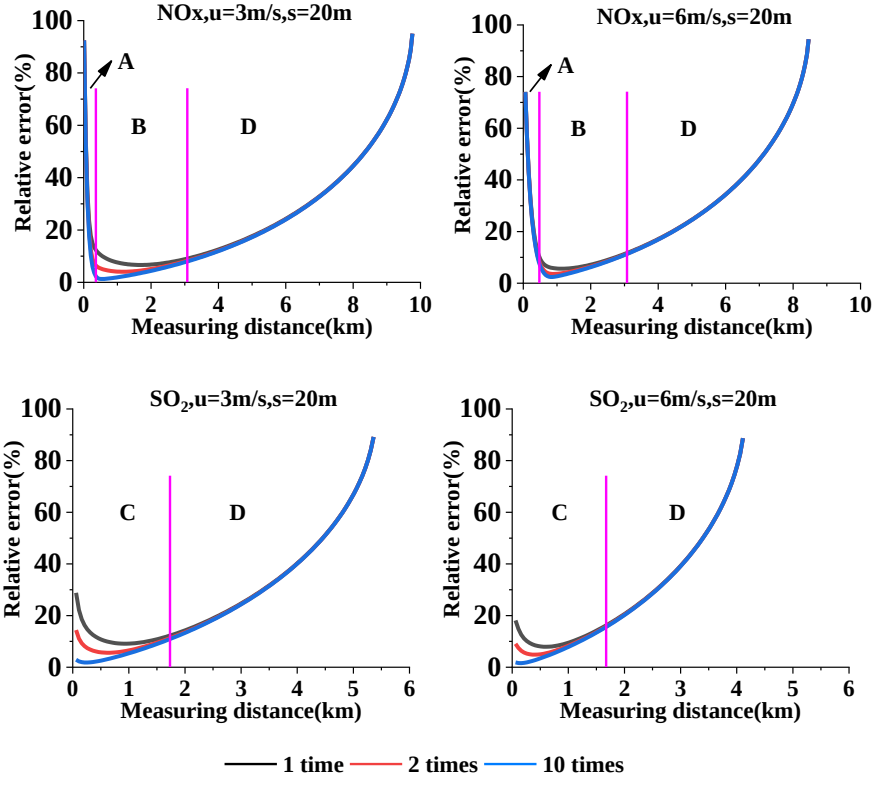

Figure 15. Emission flux error under different numbers of scans. Range A is very close to the source, range B is not too close or too far, range C is close to the source, and D is far from the source (Q = 100 g/s).

4.7 Effect of spectrometer integration times

Spectrometer noise is the main noise source of the mobile DOAS instrument (Platt and Stutz, 2008; Danckaert et al., 2015). The noise level varies under different integration times, thereby changing the retrieval error and detection limit, which would then affect the flux measurement error. Therefore, this section is focused on the effect of spectrometer integration times on mobile

https://doi.org/10.5194/amt-2020-81
Preprint. Discussion started: 15 April 2020


Atmospheric Measurement Techniques Discussions

598 DOAS flux measurement error.

599 The relationships among retrieval error, detection limit, and noise level are (Kraus, 2006;
600 Platt and Stutz, 2008)

601 $$VCD_{err} \propto Fit_{err} \propto \sigma, \quad D_{\lim} \propto \sigma \tag{21}$$

602 where VCD_{err} is the VCD retrieval error, Fit_{err} is the total fitting error in DOAS fitting, $D_{\lim}$
603 is the detection limit, and σ is the noise level. The noise level is approximately inversely
604 proportional to the square root of the integration times.

605 The sampling resolution of mobile DOAS can be expressed as:

606 $$s = v \cdot (t_s \cdot n) = v \cdot t_{\text{int}} \tag{22}$$

607 where v is the car speed, t_s is a single integration time of the spectrometer, n is the spec-
608 trometer averaging times, and t_{int} is the spectrometer integration times.

609 According to Eq. (22), the effect of integration times can be investigated in 2 different ways:
610 Varying the car speed and thus fixing the sampling resolution or fixing the car speed and thus
611 varying the sampling resolution. In this study, we simulated the integration times for $0.25\,t_{\text{int}}$,
612 $0.5\,t_{\text{int}}$, $1\,t_{\text{int}}$, $2\,t_{\text{int}}$ and $4\,t_{\text{int}}$.

613 **4.7.1 Prescribed sampling resolution**

614 Since different integration times results in the car speed varying in a large range that car
615 speed cannot be fully realized in actuality at a given sampling resolution, the sampling resolu-
616 tion cannot be too small. Here, we chose a 50 m sampling resolution as a case study.

617 Figure 16 displays the relative error under different integration times at a given sampling
618 resolution (Q = 100 g/s). From Figure 16 we can see the relative error differences resulting from
619 various integration times.

620 Since a larger integration times will directly lead to a lower detection limit and a smaller
621 fitting error, and indirectly to a lower undetectable flux and a lower retrieval error, the relative
622 error nonlinearly decreases with increasing integration times. Since the relative error differ-
623 ences caused by integration times become more evident when far from the source (range B in

https://doi.org/10.5194/amt-2020-81
Preprint. Discussion started: 15 April 2020

Atmospheric Measurement Techniques Discussions

Figure 16), our analysis focused on this range. This phenomenon is due to that fact that different integration times mainly act on the retrieval error and the detection limit. Therefore, we separately analyzed these 2 error sources.

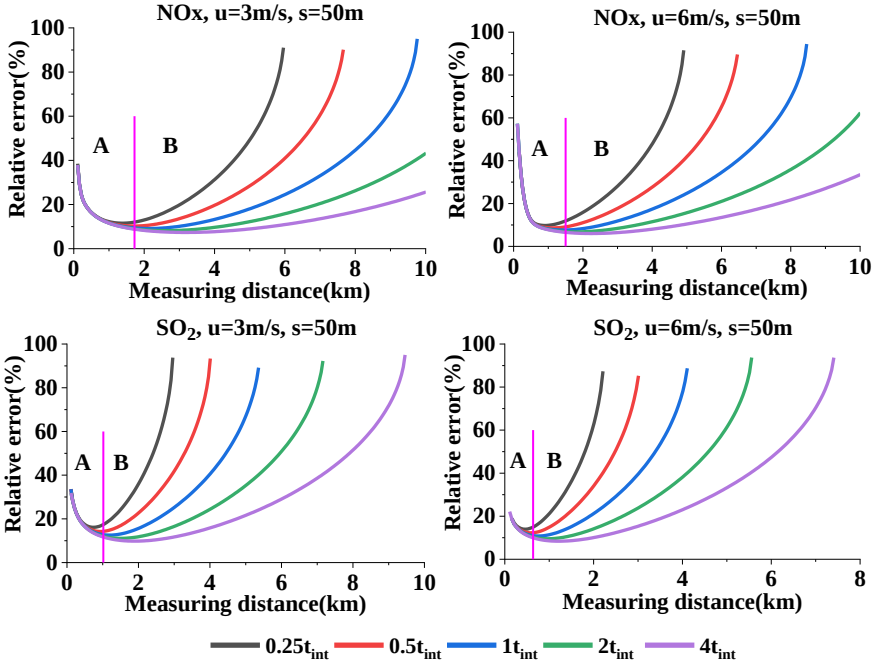

Figure 16. Relative error under different integration times at a prescribed sampling resolution (Q = 100 g/s)

First, we analyzed the flux error resulting from the retrieval error. Figure 17 presents the R^2 values of the retrieval error. These R^2 values are all < 0.12, demonstrating that retrieval error is not the main error source and, furthermore, indicating that the main reason for the relative error variation in Figure 16 should not be attributed to retrieval error.

Second, we analyzed the undetectable flux differences resulting from different detection limits. Figure 18 presents the undetectable flux and its R^2 values. From the R^2 values we could infer that undetectable flux contributes most to the error when far from the source. Especially for smaller integration times, undetectable flux R^2 increases very quickly with distance. In addition, the variation trend of undetectable flux in range B also corresponds to the relative error trend. Therefore, we infer that the relative error trend under different integration times is determined by the undetectable flux.

In brief, different integration times significantly impact the relative error at a given sampling

https://doi.org/10.5194/amt-2020-81
Preprint. Discussion started: 15 April 2020

Atmospheric Measurement Techniques Discussions

643 resolution in range B, and these error differences are mainly attributed to the undetectable flux
644 differences resulting from the detection limit.

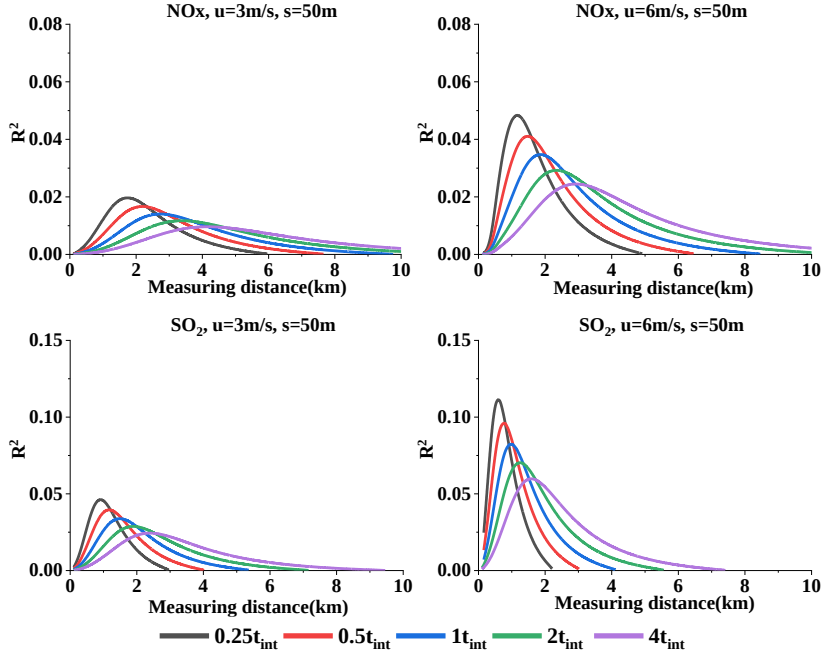

645
646
647
648 Figure 17. R^2 and flux error resulting from the retrieval error under different integration times.

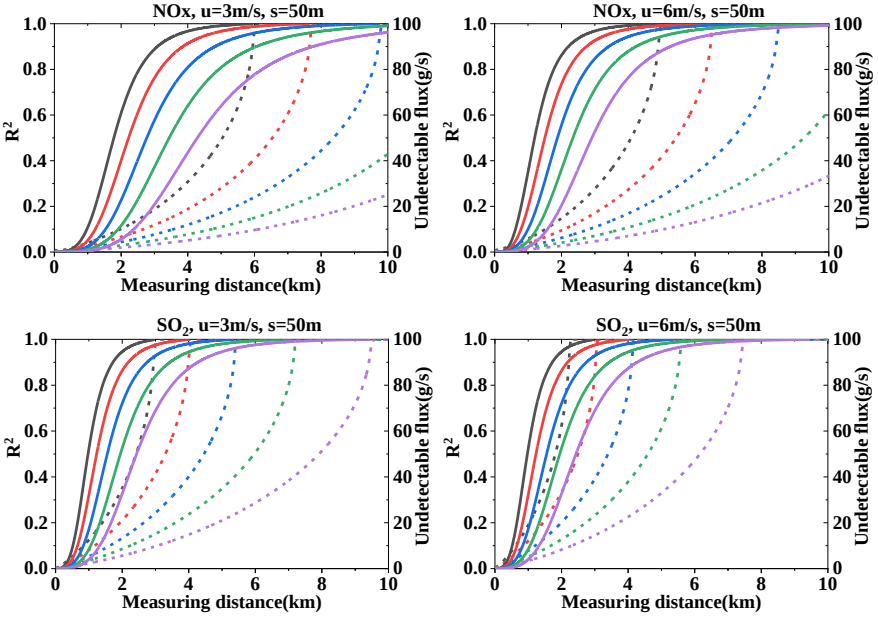

649
650

https://doi.org/10.5194/amt-2020-81
Preprint. Discussion started: 15 April 2020

Atmospheric Measurement Techniques Discussions

Figure 18. Undetectable flux and its R^2 values under wind speeds of 3 m/s and 6 m/s for NOx and SO_2 under different integration times. The sampling resolution is 50 m (Q = 100 g/s).

4.7.2. Prescribed car speed

When the car speed is prescribed, the sampling resolution is determined by the integration times integration times. Therefore, an effect on the error due to the sampling resolution would be introduced (Section 4.1).

Figure 19 presents the relative error under different integration times at a given car speed. It is interesting that the relative error differences caused by integration times in ranges B and D (NOx) are opposite those of ranges C and D (SO_2). We analyzed the causes of the relative error differences in range D, but did not analyze the causes in range B or C.

From Section 4.1 we know that, within the proper resolution range, the relative error increases with increasing sampling resolution. Moreover, the sampling resolution can only affect the first type of error source mentioned in Section 4.6, i.e., the wind field uncertainty, and retrieval error. We calculated the sum of the R^2 values for the wind field uncertainty, and retrieval error. In addition, the sum of the absolute flux errors introduced by these error sources is shown in Figure 20. The R^2 values indicate that, in range B or C, these factors are the main error source and thus cause the differences under different t_{int}. The flux error trends do not all correspond to the relative error trend due to the undetectable flux, although it is still the main error source that determines the differences in range B or C.

Furthermore, we can conclude that the different integration times that significantly affect the relative error at a given car speed can be divided into 2 ranges: B and D for NOx, and C and D for SO_2. In range B/C, the differences under different t_{int} can be attributed to the sampling resolution effect. In range D, the differences under different t_{int} can be attributed to the undetectable flux.

https://doi.org/10.5194/amt-2020-81
Preprint. Discussion started: 15 April 2020

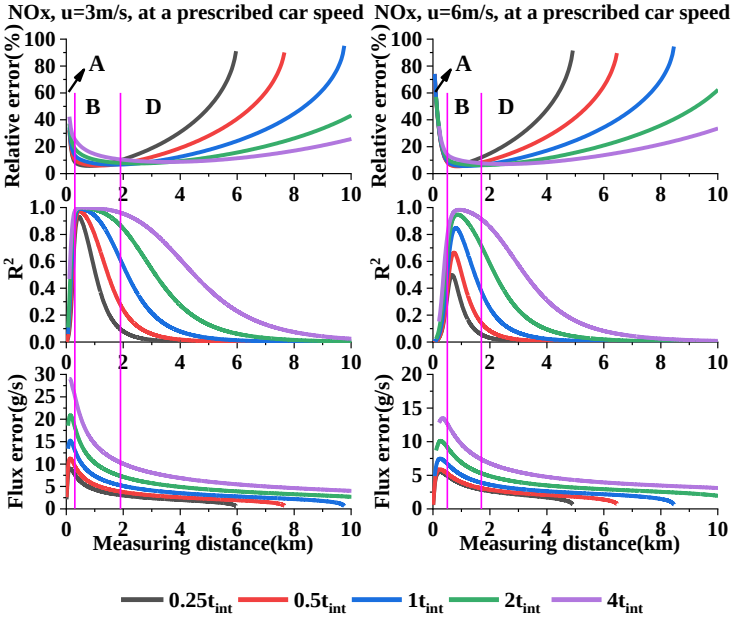

Figure 19. NOx relative errors, R^2 values, and flux errors introduced by the wind field uncertainty, and retrieval error under wind speeds of 3 m/s and 6 m/s (Q = 100 g/s)

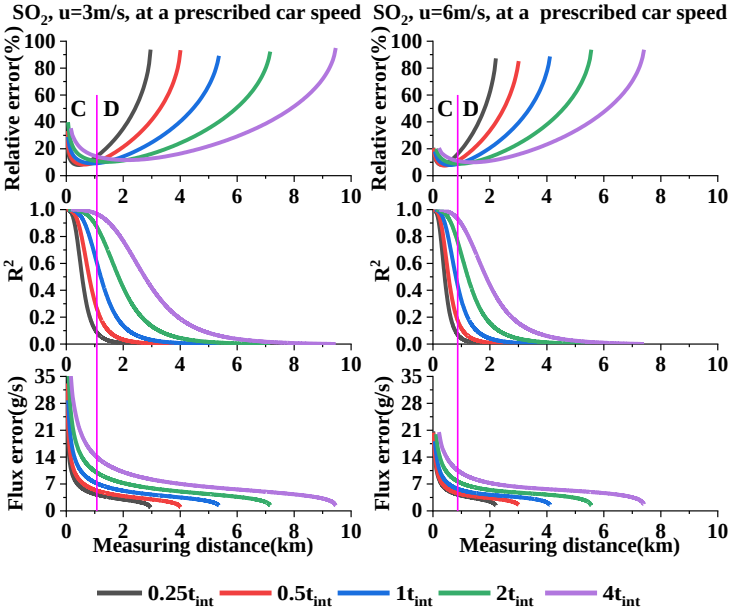

Figure 20. SO_2 relative errors, R^2 values, and flux errors introduced by the wind field uncertainty, GPS error, and retrieval error under wind speeds of 3 m/s and 6 m/s (Q = 100 g/s)

Different integration times result in different retrieval errors and different detection limits. The

https://doi.org/10.5194/amt-2020-81
Preprint. Discussion started: 15 April 2020


Atmospheric Measurement Techniques Discussions

analysis in terms of either a given sampling resolution or a given car speed has significant implications. For example, when measuring close to the source, i.e., range B or C in Figures 20 and 21, we can fix the car speed within a proper low integration times in order to obtain a higher resolution, which indirectly results in a lower error. When measuring far from the source, proper large sampling resolutions are available since the main error source is the undetectable flux. This further suggests that larger integration times and higher car speeds can be applied in order to increase the efficiency of measuring flux.

4.8 Effects from other factors

Measuring emission flux is extremely complex. It is feasible to analyze the error caused by some key factors, but it is also necessary to study other factors.

4.8.1 Emission rate

Emission rate is an objective factor. The simulation results suggest that the emission rate significantly affects the relative error distribution. Therefore, disregarding the emission rate in order to analyze the error is a less rigorous approach.

From Eqs. (10), (11), and (12) we know that VCD(x,y) is proportional to the emission rate, which means that lower emission rates generate lower VCD(x,y) levels, leading to variations of plume width and detectable flux with distance. Ultimately, this results in larger emission flux errors at the same distance when the emission rate is low, even if there is no proper resolution to measure. In order to achieve a low emission flux error, emission rates that are too low are not recommended. We cannot provide a precise lower limit for the emission rate, but can propose a range of values. From the figures in the Appendix, we can see that the red areas (indicating large errors) cover nearly all of the figure when the NOx emission rate is < 30 g/s and the SO_2 emission rate is < 50 g/s. Therefore, emission rates < 30 g/s for NOx and < 50 g/s for SO_2 are not recommended in mobile DOAS measurements.

4.8.2 Different source heights

The mobile DOAS height, which is approximately 2 m from the ground to the telescope, is usually negligible in actual measurements. When the source is not very high, however, more gas will descend to the ground under the mobile DOAS telescope, where it cannot be measured.

https://doi.org/10.5194/amt-2020-81
Preprint. Discussion started: 15 April 2020

Atmospheric Measurement Techniques Discussions

714 Here, we simulated the emission source at heights of 10 m, 20 m, 50 m, 100 m, and 200 m.
715 Since lower wind speeds will lead to gas quickly descending to the ground, we simulated a low
716 wind speed of 3 m/s. The emission rate was set to 100 g/s.

717 The lower the source height, the more gas will descend to the ground, resulting in changes
718 to the undetectable flux. Figure 21 displays the undetectable flux of NOx and SO_2 for the wind
719 speed of 3 m/s. From this figure we can see that the undetectable flux of NOx exhibits little
720 variation, while obvious variations occur in the SO_2 flux when close to the source. The unde-
721 tectable flux variation may impact the flux relative error.

722 Figure 22 presents the flux relative error at different heights. These results show that the
723 relative errors of NOx and SO_2 exhibit little variation. This is because, compared to the flux
724 error resulting from other main error sources, the undetectable flux variation with height is
725 negligible.

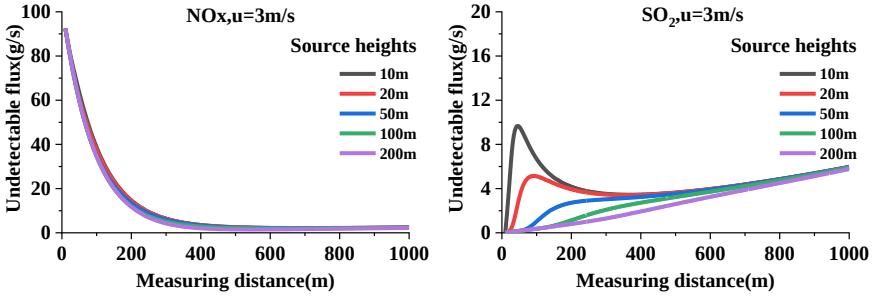

726
727 Figure 21. NOx and SO_2 undetectable flux values at different source heights (Q = 100 g/s, u = 3 m/s)

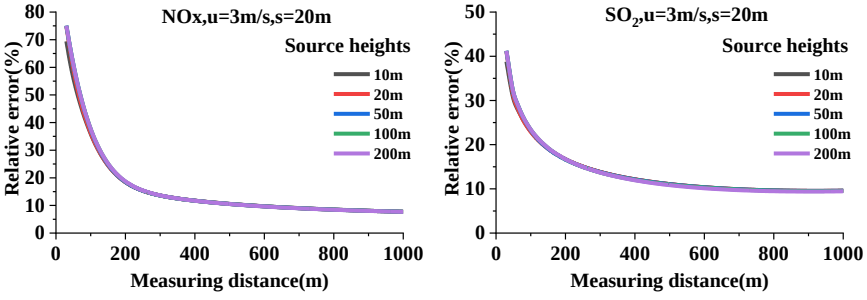

728
729 Figure 22. NOx and SO_2 flux relative errors at different source heights (Q = 100 g/s, u = 3 m/s, *s* = 20 m)

730 **4.8.3 Uncertainties of the Gaussian dispersion model**

731 The Gaussian dispersion model was assumed in the forward model during our discussion of
732 the emission flux error budget. The dispersion in actual measurements, however, depends on

https://doi.org/10.5194/amt-2020-81
Preprint. Discussion started: 15 April 2020

733 meteorological conditions and surrounding terrain. Differences in the Gaussian dispersion
734 model from reality could have resulted in a bias of the error budget presented in this study from
735 reality. The investigation of the detailed of the dispersion model is outside the scope of this
736 investigation.

737 **5 Conclusions**

738 In this study, we used a Gaussian dispersion model to quantify the NOx and SO_2 point source
739 emission flux errors of mobile DOAS.

740 We first established a forward model for the simulation.

741 In the forward model, we modified the Gaussian dispersion model in order to make it appro-
742 priate for the DOAS technique, i.e., the SO_2 and NOx VCD dispersion model. The NOx VCD
743 dispersion model also took NOx atmospheric chemical reactions into consideration.

744 Second, we analyzed the simulation data, reaching the following conclusions:

745 **(1)** The impact of sampling resolution on emission flux error is noticeable. Smaller resolution
746 can lower the flux error. In terms of measurement efficiency, the sampling resolution should be
747 moderate. Therefore, we recommended the proper sampling resolution to range from 5–50 m.
748 Larger resolutions could also be applied, but > 100 m is not recommended.

749 **(2)** Measuring distance significantly affects the flux measurement error. When far from the
750 source, undetectable flux from the wind dispersion effect, which results in large errors, will be
751 noticeable. When close to the emission source, a low number of sampling data leads to large
752 flux errors. The proper measuring distance is not too far or too close to the source. Due to the
753 complex situation, the proper distance is difficult to quantify. It should be noted that undetect-
754 able flux is the error source which was not considered in (Johansson et al., 2008, 2009; Rivera
755 et al., 2009, 2012; Ibrahim et al., 2010; Shaiganfar et al., 2011, 2017; Berg, et al.,2012; Walter,
756 2012 et al.; Wu et al., 2013, 2017; Frins et al., 2014; Merlaud et al., 2018).

757 **(3)** The wind field influence could be classified into 2 parts: uncertainty and dispersion. Dis-
758 persion is more evident when far from the emission source; thus, undetectable flux is the main
759 error source for both SO_2 and NOx. When measuring close to the emission source, wind field
760 uncertainty is the main error source of SO_2 flux measurements, but not of NOx. For higher wind

https://doi.org/10.5194/amt-2020-81
Preprint. Discussion started: 15 April 2020


Atmospheric Measurement Techniques Discussions

speeds the dispersion effect is more distinct, thereby directly leading to more undetectable flux. We recommended a wind speed of 1–4 m/s for accurate mobile DOAS measurements.

(4) NO converts to NO_2 upon exhaust from a stack and reaches the NOx steady state within a few minutes. During this time period the [NOx]/[NO_2] ratio decreases continuously with distance, resulting in a flux error due to [NOx]/[NO_2] ratio correction. Our simulation indicates that [NOx]/[NO_2] ratio correction is the main error source when measuring very close to the emission source. To minimize the large [NOx]/[NO_2] ratio correction error, we recommended $r_{NO2} = 0.05 r_{\max}$ as the NOx steady state. Therefore, the proper starting measurement distance for NOx could be determined, which we displayed in Figure 13.

(5) Retrieval error is not a dominant error source and its error budget varies with the measuring distance.

(6) Repeating the measurements several times can only affect the measurable error source, and do not affect the unmeasurable. This causes the SO_2 flux error to decrease when not very far from the emission source. As for NOx, increasing the number of measurement times could become effective when not very close to the source but not too far away.

(7) Different integration times result in different retrieval errors and detection limits. For a prescribed sampling resolution, relative error differences under different integration times are attributed to undetectable flux differences caused by the detection limit, especially for distant measurements. For a prescribed car speed, the sampling resolution effect is introduced. When measuring not very far from the emission source, the relative error differences are attributed to the sampling resolution effect from the first type of error source. Far from the source, the detection limit applies.

(8) Other studies have indicated that emission rates < 30 g/s for NOx and < 50 g/s for SO_2 are not recommended in mobile DOAS measurements. The source height exerts an impact on the undetectable flux, but has little impact on the total error.

The advantage of the method put forth in this study is that many scenarios can be simulated. Through this simulation method, we discovered a missing error source, and were able to examine the error sources and influence factors affecting flux error in more detail. Also important is

https://doi.org/10.5194/amt-2020-81
Preprint. Discussion started: 15 April 2020


Atmospheric Measurement Techniques Discussions

that the [NOx]/[NO_2] ratio correction effect of flux measurement was clarified.

Data availability. The data used in this analysis are available from the authors upon request.

Author contributions. Ang Li, Thomas Wagner and Yeyuan Huang developed the simulation method. Yeyuan Huang, Yang Wang and Zhaokun Hu designed the forward model. Hongmei Ren and Bing Dang processed the wind data. Pinhua Xie, Thomas Wagner, Jin Xu and Xiaoyi Fang supervised this study. Yeyuan Huang analyzed the data and wrote the paper. Yang Wang revised this paper preliminarily.

Competing interests. The authors declare that they have no competing interests.

Acknowledgements. This work was supported by National Natural Science Foundation of China (grant nos. 41775029, 91644110 and 41530644), National Key Research and Development Project of China 2018YFC0213201and 2017YFC0209902, Science and Technology Commission Shanghai Municipality Research Project 17DZ1203102.

References

Arystanbekova, N.Kh.: Application of Gaussian plume models for air pollution simulation at instantaneous emissions. Mathematics and Computers in Simulation, 67, 4-5. https://doi.org/10.1016/j.matcom.2004.06.023, 2004.

Bobrowski, N., Honninger, G., Galle, B., and Platt U.: Detection of bromine monoxide in a volcanic plume, Nature, 423, 273–276,2003.

Beirle, S., Hörmann, C., Penning de Vries, M., Dörner, S., Kern, C., and Wagner, T.: Estimating the volcanic emission rate and atmospheric lifetime of SO_2 from space: a case study for Kīlauea volcano, Hawai`i, Atmos. Chem. Phys., 14, 8309–8322, https://doi.org/10.5194/acp-14-8309-2014, 2014.

Beirle, S., Platt, U., Wenig, M., and Wagner, T.: Weekly cycle of NO_2 by GOME measurements: a signature of anthropogenic sources, Atmos. Chem. Phys., 3, 2225–2232, https://doi.org/10.5194/acp-3-2225-2003, 2003.

Berg, N., Mellqvist, J., Jalkanen, J.-P., and Balzani, J.: Ship emissions of SO_2 and NO_2: DOAS

https://doi.org/10.5194/amt-2020-81
Preprint. Discussion started: 15 April 2020

measurements from airborne platforms, Atmos. Meas. Tech., 5, 1085–1098, https://doi.org/10.5194/amt-5-1085-2012, 2012.

Danckaert, T., Fayt, C., van Roozendael, M., de Smedt, I., Letocart, V., Merlaud, A., and Pinardi, G.: QDOAS Software user manual, available at: http://uv-vis.aeronomie.be/software/QDOAS/QDOAS_manual.pdf (last access: 9 September 2016), 2015.

de Visscher, Alex.: AIR DISPERSION MODELING Foundations and Applications, ISBN 978-1-118-07859-4, Wiley, New York, 2014.

Ding, J., van der A, R. J., Mijling, B., Levelt, P. F., and Hao, N.: NOx emission estimates during the 2014 Youth Olympic Games in Nanjing, Atmos. Chem. Phys., 15, 9399–9412, https://doi.org/10.5194/acp-15-9399-2015, 2015.

Edmonds, M., Herd, R. A., Galle, B., and Oppenheimer, C. M.: Automated high-time resolution measurements of SO_2 flux at Soufrière Hills Volcano, Montserrat, B. Volcanol., 65, 578–586, 2003.

Frins, E., Bobrowski, N., Osorio, M., Casaballe, N., Belsterli, G., Wagner, T. and Platt, U.: Scanning and mobile Multi-Axis DOAS measurements of SO_2 and NO_2 emissions from an electric power plant in Montevideo, Uruguay. Atmos. Environ., 98, 347–356. https://doi.org/10.1016/j.atmosenv.2014.03.069, 2014.

Galle, B., Oppenheimer, C., Geyer, A., McGonigle, A.J.S., Edmonds, M. and Horrocks, L.: A miniaturized ultraviolet spectrometer for remote sensing of SO_2 fluxes: A new tool for volcano surveillance. J. Volcanol. Geother. Res., 119, 241–254, 2003.

Hönninger, G., von Friedeburg, C., and Platt, U.: Multi axis differential optical absorption spectroscopy (MAX-DOAS), Atmos. Chem. Phys., 4, 231–254, https://doi.org/10.5194/acp-4-231-2004, 2004.

Ibrahim, O., Shaiganfar, R., Sinreich, R., Stein, T., Platt, U., and Wagner, T.: Car MAX-DOAS measurements around entire cities: quantification of NOx emissions from the cities of Mannheim and Ludwigshafen (Germany), Atmos. Meas. Tech., 3, 709–721, https://doi.org/10.5194/amt-3-709-2010, 2010.

https://doi.org/10.5194/amt-2020-81
Preprint. Discussion started: 15 April 2020

844 Jin, J., Ma, J., Lin, W., Zhao, H., Shaiganfar, R., Beirle, S., and Wagner, T.: MAX-DOAS meas-
845 urements and satellite validation of tropospheric NO_2 and SO_2 vertical column densities at a
846 rural site of North China, Atmos. Environ., 133, 12–25, https://doi.org/10.1016/j.at-
847 mosenv.2016.03.031, 2016.
848 Johansson, M., Rivera, C., de Foy, B., Lei, W., Song, J., Zhang, Y., Galle, B., and Molina, L.:
849 Mobile mini-DOAS measurement of the outflow of NO_2 and HCHO from Mexico City, At-
850 mos. Chem. Phys., 9, 5647–5653, https://doi.org/10.5194/acp-9-5647-2009, 2009.
851 Johansson, M., Galle, B., Yu, T., Tang, L., Chen, D., Li, H., Li, J., Zhang, Y.: Quantification of
852 total emission of air pollutants from Beijing using mobile mini-DOAS. Atmos. Environ.,
853 42,6926–6933. https://doi.org/10.1016/j.atmosenv.2008.05.025, 2008.
854 Kraus, S.: DOASIS, A Framework Design for DOAS, PhD thesis, University of Mannheim
855 (http://hci.iwr.uni-heidelberg.de/publications/dip/2006/Kraus PhD2006.pdf), 2006.
856 Lushi, E., Stockie, J. M.: An inverse Gaussian plume approach for estimating atmospheric pol-
857 lutant emissions from multiple point sources. Atmos. Environ., 44, 1097-1107.
858 https://doi.org/10.1016/j.atmosenv.2009.11.039, 2009.
859 Merlaud, A., Tack, F., Constantin, D., Georgescu, L., Maes, J., Fayt, C., Mingireanu, F.,
860 Schuettemeyer, D., Meier, A. C., Schönardt, A., Ruhtz, T., Bellegante, L., Nicolae, D., Den
861 Hoed, M., Allaart, M., and Van Roozendael, M.: The Small Whiskbroom Imager for atmos-
862 pheric compositioN monitorinG (SWING) and its operations from an unmanned aerial vehi-
863 cle (UAV) during the AROMAT campaign, Atmos. Meas. Tech., 11, 551–567,
864 https://doi.org/10.5194/amt-11-551-2018, 2018.
865 Platt, U. and Stutz, J.: Differential Optical Absorption Spectroscopy (DOAS), Principles and
866 Applications, ISBN 978-3-540-21193-8, Springer, Berlin-Heidelberg, 2008.
867 Richter, A., Burrows, J. P., Nüß, H., Granier, C., and Niemeier, U.: Increase in tropospheric
868 nitrogen dioxide over China observed from space, Nature, 437, 129–132, 2005.
869 Rivera, C., Sosa, G., Wöhrnschimmel, H., de Foy, B., Johansson, M., and Galle, B.: Tula indus-
870 trial complex (Mexico) emissions of SO_2 and NO_2 during the MCMA 2006 field campaign
871 using a mobile mini-DOAS system, Atmos. Chem. Phys., 9, 6351–6361,

https://doi.org/10.5194/amt-2020-81
Preprint. Discussion started: 15 April 2020

https://doi.org/10.5194/acp-9-6351-2009, 2009.

Seinfeld, J. H. and Pandis, S. N.: Atmospheric Chemistry and Physics – From Air Pollution to Climate Change, John Wiley, New York, 1998.

Shaiganfar, R., Beirle, S., Sharma, M., Chauhan, A., Singh, R. P., and Wagner, T.: Estimation of NOx emissions from Delhi using Car MAX-DOAS observations and comparison with OMI satellite data, Atmos. Chem. Phys., 11, 10871–10887, https://doi.org/10.5194/acp-11-10871-2011, 2011.

Shaiganfar, R., Beirle, S., Denier van der Gon, H., Jonkers, S., Kuenen, J., Petetin, H., Zhang, Q., Beekmann, M., and Wagner, T.: Estimation of the Paris NOx emissions from mobile MAX-DOAS observations and CHIMERE model simulations during the MEGAPOLI campaign using the closed integral method, Atmos. Chem. Phys., 17, 7853–7890, https://doi.org/10.5194/acp-17-7853-2017, 2017.

Spicer, C. W.: Nitrogen Oxide Reactions in the Urban Plume of Boston. Science, 215, 1095–1097. http://www.sciencemag.org/cgi/doi/10.1126/science.215.4536.1095, 1982.

Wagner, T., Dix B., Friedeburg, C. v., Frieß, U., Sanghavi, S., Sinreich, R., and Platt, U.: MAX-DOAS O_4 measurements –a new technique to derive information on atmospheric aerosols - Principles and information content, J. Geophys. Res., 109, D22205, https://doi.org/10.1029/2004JD004904, 2004.

Wagner, T., Ibrahim, O., Shaiganfar, R., and Platt, U.: Mobile MAX-DOAS observations of tropospheric trace gases, Atmos. Meas. Tech., 3, 129–140, https://doi.org/10.5194/amt-3-129-2010, 2010.

Wagner, T., Beirle, S., Brauers, T., Deutschmann, T., Frieß, U., Hak, C., Halla, J. D., Heue, K. P., Junkermann, W., Li, X., Platt, U., and Pundt-Gruber, I.: Inversion of tropospheric profiles of aerosol extinction and HCHO and NO_2 mixing ratios from MAX-DOAS observations in Milano during the summer of 2003 and comparison with independent data sets, Atmos. Meas. Tech., 4, 2685–2715, https://doi.org/10.5194/amt-4-2685-2011, 2011.

Walter, D., Heue, K. P., Rauthe‐Schöch, A., Brenninkmeijer, C. A. M., Lamsal,L. N., Krotkov, N. A. Platt, U.: Flux calculation using CARIBIC DOAS aircraft measurements: SO_2 emission

https://doi.org/10.5194/amt-2020-81
Preprint. Discussion started: 15 April 2020

Atmospheric Measurement Techniques Discussions

of Norilsk, J. Geophys. Res., 117, D11305, https://doi.org/10.1029/2011JD017335, 2012.

Wu, F. C., Xie, P. H., Li, A., Chan, K. L., Hartl, A., Wang, Y., Si, F. Q., Zeng, Y., Qin, M., Xu, J., Liu, J. G., Liu, W. Q., and Wenig, M.: Observations of SO_2 and NO_2 by mobile DOAS in the Guangzhou eastern area during the Asian Games 2010, Atmos. Meas. Tech., 6, 2277–2292, https://doi.org/10.5194/amt-6-2277-2013, 2013.

Wu, F., Xie, P., Li, A., Mou, F., Chen, H., Zhu, Y., Zhu, T., Liu, J., and Liu, W.: Investigations of temporal and spatial distribution of precursors SO_2 and NO_2 vertical columns in the North China Plain using mobile DOAS, Atmos. Chem. Phys., 18, 1535–1554, https://doi.org/10.5194/acp-18-1535-2018, 2018.

Appendix

1. NOx simulation results (relative error)

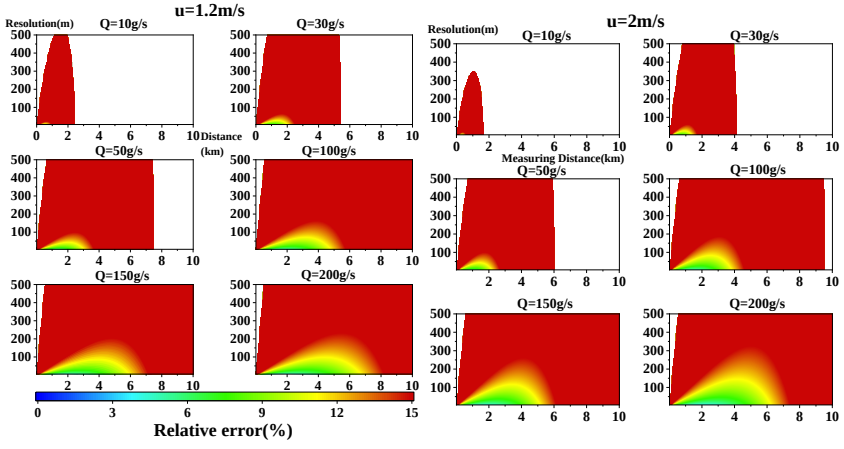

https://doi.org/10.5194/amt-2020-81
Preprint. Discussion started: 15 April 2020

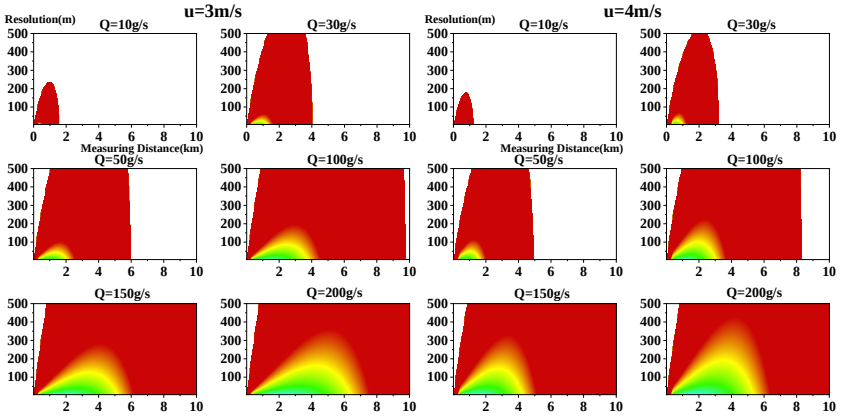

913

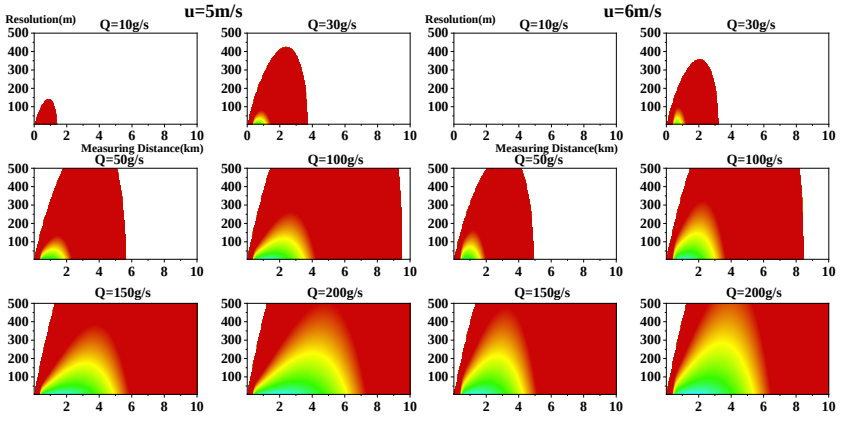

914

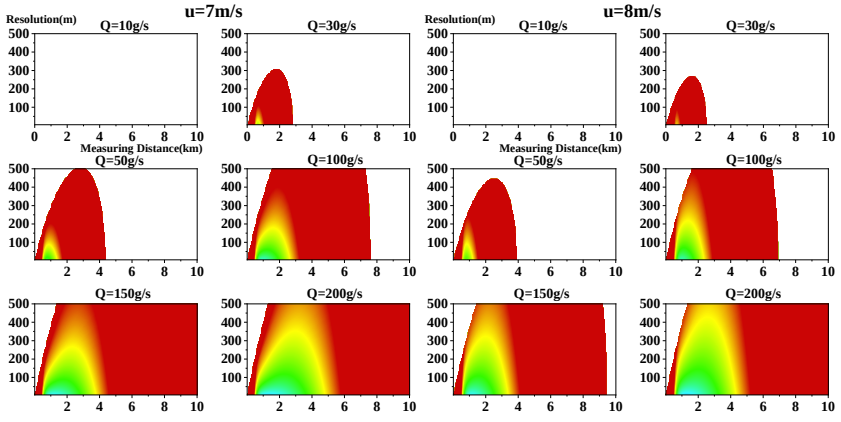

915
916

917 Figure 23. Relative errors (using Eq. 19) of NOx as a function of the measurement distance from the source
918 (*x*-axis) and the sampling resolution (*y*-axis). The different subfigures show the results for different wind

https://doi.org/10.5194/amt-2020-81
Preprint. Discussion started: 15 April 2020

Atmospheric Measurement Techniques Discussions

speeds and different emission rates. The color map indicates the relative errors.

2. SO_2 simulation results (relative error)

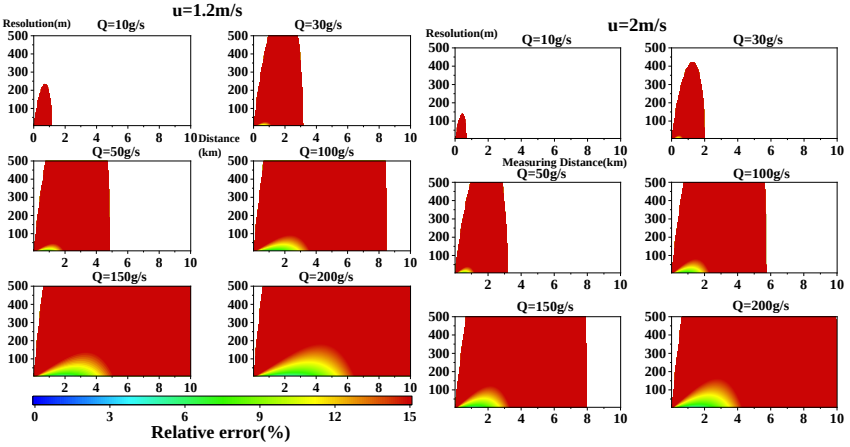

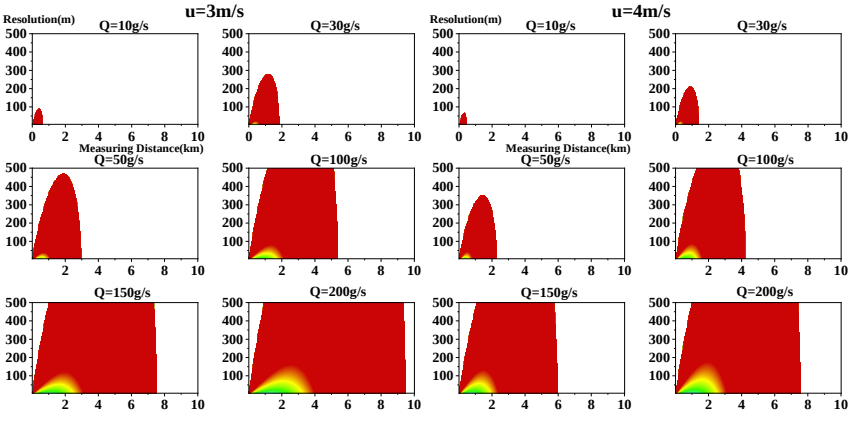

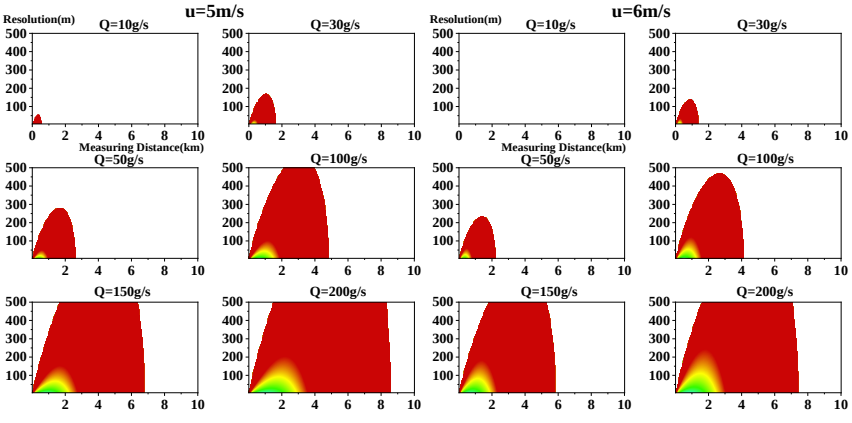

https://doi.org/10.5194/amt-2020-81
Preprint. Discussion started: 15 April 2020

Atmospheric Measurement Techniques Discussions

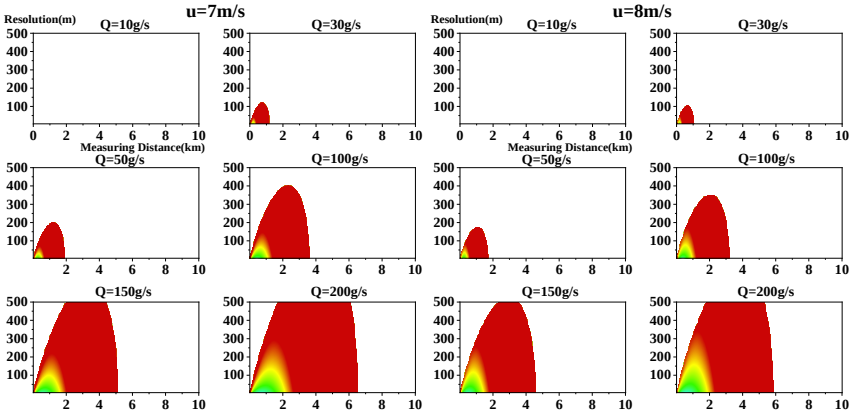

924

925 Figure 24. Relative error (using Eq. 18) of the distribution of SO_2 for different wind fields of different
926 emission rates. The unit of all abscissas is the measurement distance from the source (km), while that
927 of the ordinate is the sampling resolution (m). The color map indicates the relative errors.